

FINDS: Mitsubishi PWR Fuel Assemblies

Seismic Analysis Code

Non-Proprietary Version

March 2008

© 2008 Mitsubishi Heavy Industries, Ltd.
All Rights Reserved

Revision History

Revision	Page	Description
0	All	Original issued

© 2008
MITSUBISHI HEAVY INDUSTRIES, LTD.
All Rights Reserved

This document has been prepared by Mitsubishi Heavy Industries, Ltd. (MHI) in connection with the U.S. Nuclear Regulatory Commission ("NRC") licensing review of the US-APWR nuclear power plant design. No right to disclose, use or copy any of the information in this document, other than by the NRC and its contractors in support of the licensing review of the US-APWR, is authorized without the express written permission of MHI.

This document contains MHI's technology information and intellectual property relating to the US-APWR and it is delivered to the NRC on the express condition that it not be disclosed, copied or reproduced in whole or in part, or used for the benefit of anyone other than MHI without the express written permission of MHI, except as set forth in the previous paragraph.

This document is protected by the laws of Japan, U.S. copyright law, international treaties and conventions, and the applicable laws of any country where it is being used.

Mitsubishi Heavy Industries, Ltd.
16-5, Konan 2-chome, Minato-ku
Tokyo 108-8215 Japan

Abstract

The FINDS code(*) is the Mitsubishi PWR fuel assembly seismic analysis code. The FINDS code was developed based on analytical models and data obtained from tests using Mitsubishi fuel assemblies. The resulting analytical model represents the row in the core with the maximum number of fuel assemblies in it; for instance, 17 assemblies in the US-APWR and 15 assemblies in conventional three and four loop plants. The FINDS code does a time-history analysis of the fuel assemblies' horizontal vibration including the impact of adjacent fuel assemblies, and fuel assembly and core baffle plate, and plastic deformation of the grid spacer if the impact force exceeds its elastic limit. In the early eighty's, a government sponsored project was conducted simulating seismic behavior of PWR and BWR fuel assemblies and the Mitsubishi FINDS code was verified to generate predictions consistent with the data obtained from this project.

The complex response of the fuel assemblies under seismic conditions is well predicted by the FINDS code. The code includes non-linear characteristics such as amplitude dependent damping, frequency and grid spacer deformation. Verification data for the FINDS code are included in this report.

(*) Fuel IN-elastic Deformation under Seismic condition

Table of Contents

List of Figures	iv
1.0 INTRODUCTION	1-1
2.0 THE BEHAVIOR OF FUEL ASSEMBLIES IN A PWR CORE DURING AN EARTHQUAKE	2-1
2.1 Fuel Assemblies in the Reactor	2-1
2.2 Propagation of an Earthquake Wave to the Fuel Assemblies	2-1
2.3 Vibration of the Fuel Assemblies	2-2
3.0 DESCRIPTION OF THE FINDS CODE	3-1
3.1 Multiple Vibration Model in the FINDS Code	3-1
3.2 Detailed Model of Fuel Assemblies in the FINDS Code	3-4
3.3 Fundamental Equation for Vibration of the Fuel Assembly	3-6
3.4 Mode-superposition Method	3-8
3.5 Non-linear Damping and Frequency Model	3-9
3.6 Solution Process for Non-linear Vibration	3-13
3.7 In-elastic Impact Model	3-16
3.7.1 Multi-Fuel Assembly Impact Model	3-16
3.7.2 Stiffness and Viscous Damping Coefficient in the Impact Model	3-20
3.7.3 Description of the Grid Spacer Deformation Progression	3-22
4.0 FUNDAMENTAL TESTS FOR MODELING	4-1
4.1 Large Amplitude Vibration Test of Fuel Assembly	4-1
4.2 Grid Spacer Impact and Deformation Test	4-7
4.2.1 Reduction of Characterized Data for the Deformation Progress	4-7
4.2.2 Characteristics for Half-sized Grid Spacer Region	4-12
4.3 Additional Treatment for the Analysis of the In-core Conditions	4-18
5.0 VERIFICATION OF THE FINDS CODE	5-1
5.1 Vibrational Behavior of the Beam Model	5-1
5.2 Lateral Impact Test of Fuel Assembly	5-5
5.3 Impact Tests of Single Span Fuel Assembly	5-7
5.4 Seismic Excitation Tests of Multiple Fuel Assemblies	5-11
6.0 CONCLUSION	6-1
7.0 REFERENCES	7-1
Appendix A INPUT for FINDS	
Appendix B OUTPUT from FINDS	

List of Figures

Figure 2.1-1	US-APWR Reactor Internals and Fuel Assembles General Arrangement.....	2-3
Figure 2.2-1	Typical Analysis Model of the Reactor Internals for the Seismic and LOCA Dynamic Analysis (RV, Lower Reactor Internals and CRDM).....	2-4
Figure 2.2-2	Typical Analysis Model for the Seismic and LOCA Dynamic Analysis (Fuel Assembly, Upper Reactor Internals and Diffuser Plate).....	2-5
Figure 3.1-1	Cross Section of the US-APWR Core.....	3-2
Figure 3.1-2	Model for Lateral Impacting of US-APWR Fuel Assemblies Model	3-3
Figure 3.2-1	Vibration Model for the US-APWR Fuel Assembly.....	3-5
Figure 3.5-1	Non-linear Mechanisms in a Fuel Assembly Structure.....	3-11
Figure 3.5-2	Load-Deflection Characteristics of a Fuel Assembly due to Lateral Loading.	3-11
Figure 3.5-3	Amplitude-dependent Frequency and Damping Characteristics of 1st mode	3-12
Figure 3.6-1	FINDS Code Basic Flow Diagram.....	3-15
Figure 3.7.1-1	Multi-Fuel Assembly Impact Model	3-19
Figure 3.7.2-1	Modeling of Grid Spacer Characteristics.....	3-21
Figure 3.7.2-2	Grid Spacer and Pendulum Type Impact Test	3-21
Figure 3.7.3-1	Load-Deflection Curves of Sequential Impacts	3-24
Figure 3.7.3-2	Typical Load-Deflection Curves of Two Consecutive Impacts.....	3-25
Figure 3.7.3-3	Correlations between ESC, Stiffness and Deformation.....	3-25
Figure 4.1-1	Fuel Assembly Lateral Pluck Test.....	4-2
Figure 4.1-2	Amplitude Dependent Coefficients of Natural Frequency in Air.....	4-3
Figure 4.1-3	Amplitude Dependence of Natural Frequency in Air (Assuming Constant Damping)	4-3
Figure 4.1-4	Amplitude Dependent Coefficients of Damping Factor in Air.....	4-4
Figure 4.1-5	Amplitude Dependence of Damping Factor in Air	4-4
Figure 4.1-6	Amplitude Dependence of Natural Frequency in Air.....	4-5
Figure 4.1-7	Amplitude Dependence of Natural Frequency in Still Water.....	4-6
Figure 4.1-8	Amplitude Dependence of Damping Factor in Still Water.....	4-6
Figure 4.2.1-1	Relationship between Relaxation of Stiffness and ESC	4-8
Figure 4.2.1-2	Relationship between Deformation and ESC.....	4-8
Figure 4.2.1-3	Sampling of Local Stiffness Change and Deformation Energy.....	4-9
Figure 4.2.1-4	Variation of Pendulum Angle in Simulation Test Cases	4-9
Figure 4.2.1-5	Comparison of Analyzed and Measured Impact Force	4-10
Figure 4.2.1-6	Comparison of Analyzed and Measured Plastic Deformation	4-10

Figure 4.2.1-7 Comparison of Analyzed and Measured Restitution Coefficient..... 4-11

Figure 4.2.2-1 Relationship between Reduced Stiffness and ESC for Half-sized Grid Spacer Region..... 4-16

Figure 4.2.2-2 Relationship between Plastic Deformation and ESC for Half-sized Grid Spacer Region..... 4-16

Figure 4.2.2-3 Force Distribution among Sequential Grid Spacer Cells 4-17

Figure 4.2.2-4 Deformation Distributions in Grid Spacer Model 4-17

Figure 4.3-1 Damping Factor at Hot Conditions 4-20

Figure 4.3-2 Natural Frequencies at Hot Conditions 4-20

Figure 5.1-1 Comparison between FINDS and ANSYS Codes (Accelerated by the 1st Mode frequency) 5-2

Figure 5.1-2 Comparison between FINDS and ANSYS Codes (Accelerated by the 2nd Mode frequency) 5-3

Figure 5.1-3 Comparison between FINDS and ANSYS Codes (Accelerated by the 3rd Mode frequency) 5-4

Figure 5.2-1 Impact Force 5-6

Figure 5.2-2 Rebound Displacement 5-6

Figure 5.3-1 Single Span Fuel Assembly Impact Test 5-8

Figure 5.3-2 Drop Height of the Single Span Fuel Assembly 5-8

Figure 5.3-3 Comparison of Calculated Impact Forces with Measurements 5-9

Figure 5.3-4 Comparison of Calculated Deformation of Grid Spacers with Measurements . 5-9

Figure 5.3-5 Comparison of Calculated Restitution Coefficient with Measurements..... 5-10

Figure 5.4-1 Configuration of PWR Core Internals Seismic Response Test..... 5-13

Figure 5.4-2 Displacements of the Fuel Assemblies at Both Ends of the Row 5-14

Figure 5.4-3 Grid Spacer Maximum Displacement (S_1 Wave)..... 5-15

Figure 5.4-4 Maximum Impact Force on the Fuel Assembly (S_1 Wave) 5-15

Figure 5.4-5 Vibration Behavior of the Multiple Fuel Assemblies (Time History, 0-20 Seconds, S_1 Wave)..... 5-16

Figure 5.4-6 Impact Forces and Grid Spacers' Plastic Deformation in the Fuel Assemblies at Both Ends of the Row (S_2 Wave)..... 5-17

1.0 INTRODUCTION

Mitsubishi Heavy Industries, Ltd. (Mitsubishi) has substantial experience in the nuclear industry in Japan, having supplied more than 18,000 nuclear fuel assemblies to Japanese PWR utilities since 1969. The irradiation experience accumulated for Mitsubishi fuel assemblies has demonstrated excellent performance and high reliability.

The fuel design, fabrication, the associated analysis methods and criteria that have led to the high reliability performance of Mitsubishi fuel in Japan will now be applied to the design and manufacture of US-APWR fuel, consistent with NRC regulations and standards. The US-APWR fuel incorporates the latest design such as corrosion resistant cladding, 97 % theoretical density (TD) pellets, 10 wt% gadolinia doped fuel and includes features to reduce or eliminate debris fretting, grid spacer fretting and incomplete rod insertion.

The fuel rod and fuel assembly design criteria to be applied to the US-APWR fuel design are in compliance with Title 10 of Code of Federal Regulations Part 50 (10CFR50), Regulatory Guide 1.206, and the NRC Standard Review Plan (NUREG-0800).

Since a PWR fuel assembly has a high length to width ratio, it is easy to excite horizontal vibration during an earthquake. In a PWR, fuel assemblies have small lateral gaps between them in the core, thus grid spacer impacts will occur when the vibration amplitude is larger than the gap. A more complex response occurs when the vibration results in grid spacer impacting. The structure of a PWR fuel assembly consists of several elements such as fuel rods, control rod guide thimbles, grid spacers and nozzles. The fuel rods are supported by the springs and dimples of the grid spacer and easily slide at the grid spacer locations. Therefore, the vibration of the fuel assembly will exhibit non-linear behavior. If the grid spacer impact force due to collision exceeds its elastic limit, plastic deformation will occur in the grid spacer and subsequent behavior will be accompanied by other non-linear responses.

The FINDS code development has been done to provide a comprehensive method to simulate the behavior of fuel assemblies under seismic response based on out-of pile tests using Mitsubishi PWR fuel assemblies and grid spacers. A large scale project, which was sponsored by the Japanese government to examine the response of the fuel in a PWR core under seismic conditions, demonstrated that a fuel assembly kept its integrity and control rod insertion capability even under severe seismic conditions. The FINDS code was used to predict the fuel assemblies' response during the test in terms of vibration amplitude, grid spacer impact force and grid spacer deformation, and thus verified the adequacy of the FINDS code.

The FINDS code was originally developed to analyze fuel assemblies' horizontal response under seismic conditions, but it can be also used for the analysis of fuel assemblies' horizontal response generated by pressure propagation during LOCA.

The US-APWR fuel assembly analysis methodology for combined seismic and LOCA is described in Appendix D of Reference 1. The following description is directed to the response analysis due to an earthquake. However the same methodology is applied to the LOCA analysis, with the only difference being the core plates' time histories input.

2.0 THE BEHAVIOR OF FUEL ASSEMBLIES IN A PWR CORE DURING AN EARTHQUAKE

2.1 Fuel Assemblies in the Reactor

The US-APWR fuel assemblies are loaded inside the reactor vessel as shown in Figure 2.1-1. The reactor vessel contains structures that serve to support the fuel assemblies, guide the control rods, and form paths for the coolant flow. Of the core internal structures, the upper core plate, the lower core support plate, the upper support columns, and other such structures that support the fuel assemblies are referred to as the core support structures. The fuel assemblies are supported within the core barrel by the upper core plate and the lower core support plate, and are fixed in place by pins attached to the upper core plate and the lower core support plate. In the US-APWR the fuel assemblies are also surrounded by neutron reflectors that are placed in the core periphery. Fuel assemblies in a conventional PWR reactor are supported by a lower core plate and surrounded by a core baffle plate versus a lower core support plate and neutron reflector in the US-APWR

During the plant operation, the upward hydraulic lift force and buoyant force are counteracted by gravity and the mechanical force from the fuel assembly hold-down springs to prevent liftoff of the fuel assembly. Once an earthquake happens, the additional loads, caused by a motion of the reactor vessel, act on the fuel assemblies.

2.2 Propagation of an Earthquake Wave to the Fuel Assemblies

The propagation of an earthquake wave to the fuel assembly is described below.

- Vibration of the reactor building caused by the earthquake leads to the vibration of the reactor vessel.
- The vibration of the reactor vessel is accompanied by vibration of the upper core plate and the lower core support plate that support the fuel assemblies and the neutron reflector that surround the core. Analysis models for time history response at the reactor vessel support and upper core plate/lower core support and neutron reflector are illustrated in Figure 2.2-1 and 2.2-2. These figures represent a typical analysis model of the reactor internals used for seismic analysis. The physical geometry and material properties (density, modulus of elasticity, Poisson's ratio) of the reactor internals are represented by beam elements. The reactor internals and interfacing structures are connected or represented by mass inertia effects, stiffness matrices, and hydro-dynamic matrices, springs, and/or impact elements including gap and damping (including coexistence of viscous and Coulomb damping). The nodal point degrees of freedom, and damping coefficients of the reactor internals and surrounding structures are selected such that the most dominant frequencies are represented in the seismic response. Dominant frequencies are identified by comparing the frequency response of the reactor internals with the expected responses based on experience and experiment measurements. Fluid-structure interaction effects are accounted for by matrices developed for that purpose. The reactor internals seismic input can use in-structure response spectra or in-structure time-history accelerations which are obtained from the analysis results described in Subsection 3.7.2 and Appendix 3H of Reference 2. This model is used to determine the effect of vibratory motion due to a Safe Shutdown Earthquake (SSE) and 1/3 SSE called the Operational Basis Earthquake (OBE). Additional loading inputs to the seismic analysis are the vertical pressure loadings

converted to nodal point external loads, and the vertical weights of the reactor internals and interfacing components by input of density for the beams with spring effects or mass nodal points.

- Because the upper core and the lower core support plates vibrate in both vertical and horizontal directions, the fuel assemblies supported by the plates are accelerated.

2.3 Vibration of the Fuel Assemblies

The fuel assemblies are vibrated in both horizontal and vertical directions due to the acceleration induced by the upper core and the lower core support plates.

The FINDS code analyzes the horizontal response of the multiple fuel assemblies.

The magnitude and phase of the horizontal acceleration that acts on the fuel assemblies due to the vibration of the upper and lower core support points are the same for all assemblies, because of the lateral rigidity of the core plates. Therefore, all of the fuel assemblies vibrate in synchrony. If the vibration is large, collisions with the neutron reflectors or between adjacent fuel assemblies may occur at the position of the grid spacers, which will affect the horizontal vibration behavior of each fuel assembly, and result in in-elastic deformation of the grid spacers when the impact forces are beyond the grid spacer's elastic limit.

Therefore, the FINDS code solves the fuel assembly's response considering grid spacer impacts and deformation and the vibration characteristics related to amplitude, frequency and damping, as described below.

Evaluation method for the fuel assembly response to the vertical vibration is described in Appendix D of Reference 1.

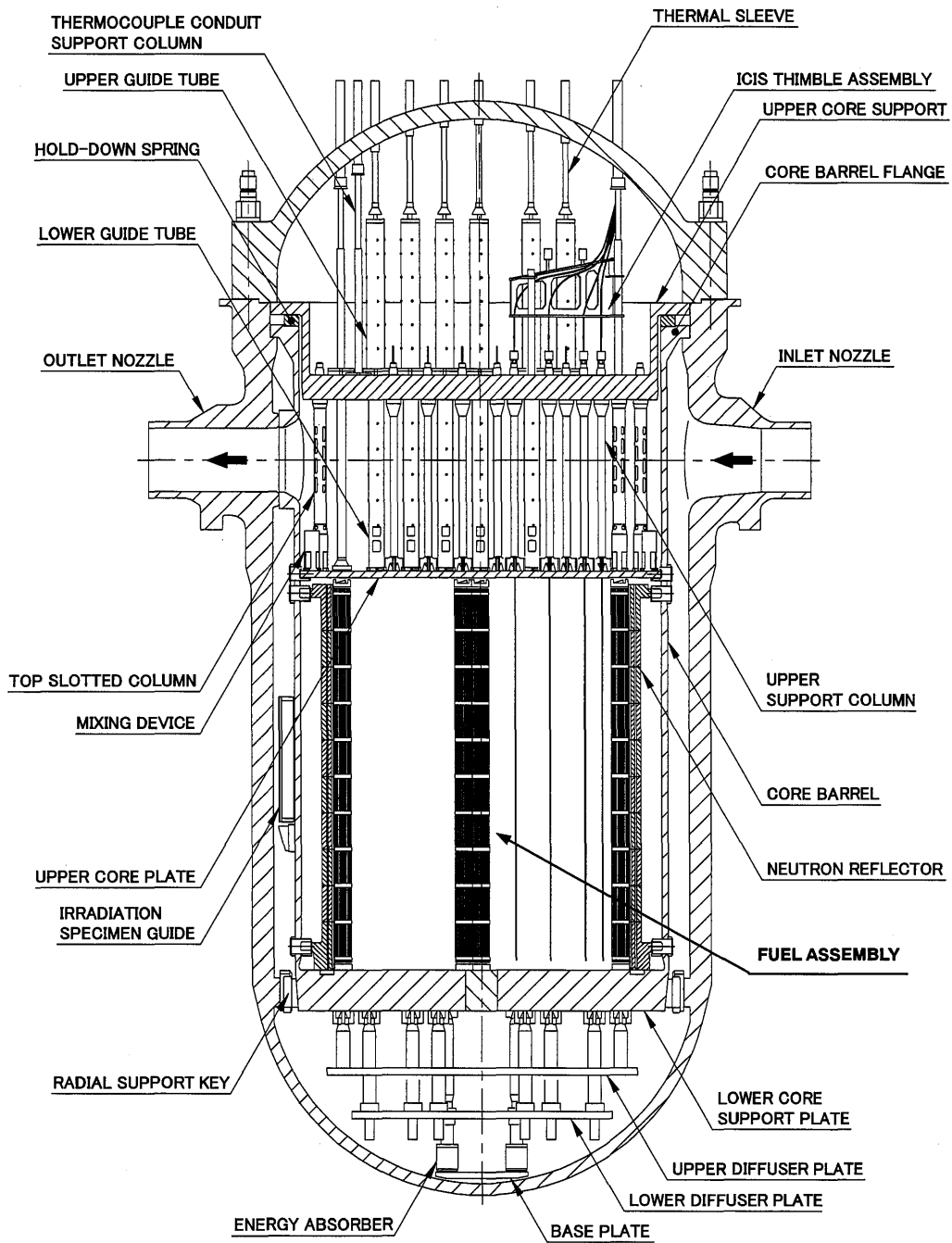


Figure 2.1-1 US-APWR Reactor Internals and Fuel Assemblies General Arrangement

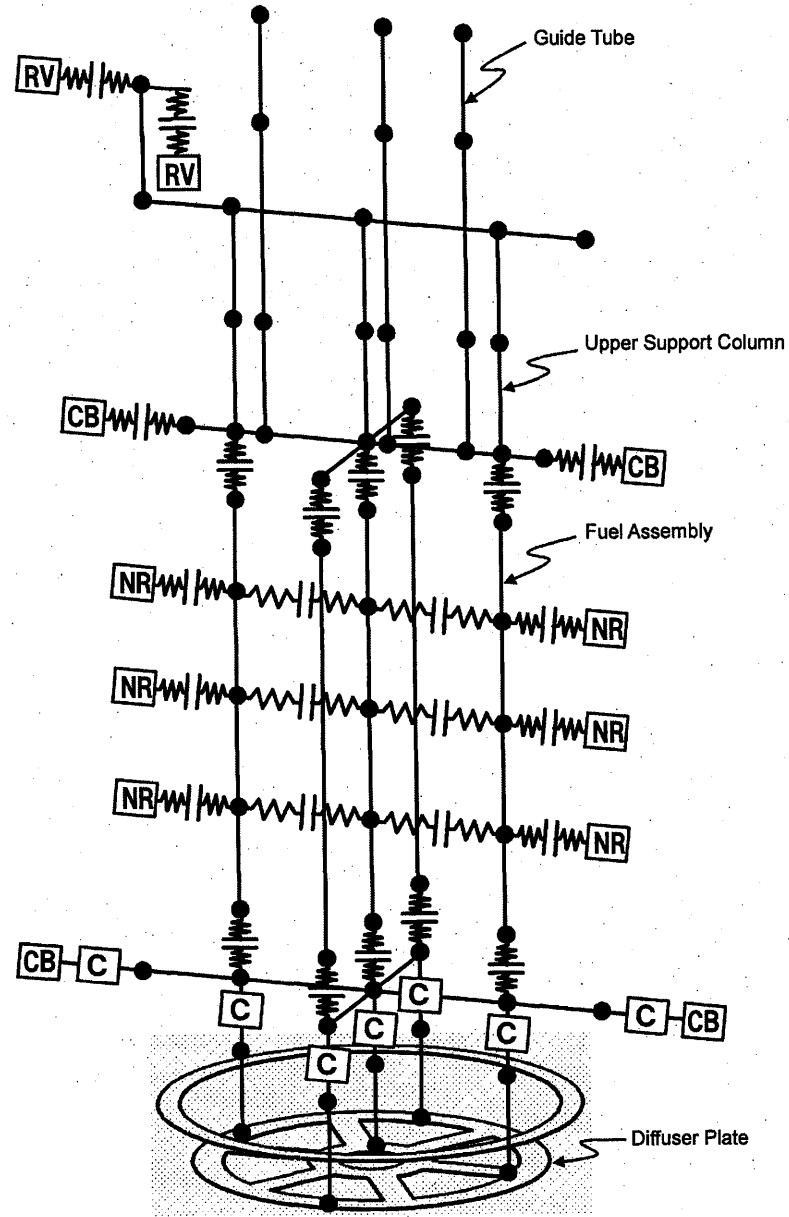


Figure 2.2-2 Typical Analysis Model for the Seismic and LOCA Dynamic Analysis (Fuel Assembly, Upper Reactor Internals and Diffuser Plate)

3.0 DESCRIPTION OF THE FINDS CODE

The theory and modeling of the FINDS code are described in the following sections. A summary may be found in Reference 3.

3.1 Multiple Vibration Model in the FINDS Code

The FINDS code analyzes the horizontal vibration response of fuel assemblies due to a seismic event using time history acceleration waves at the upper core plate and the lower core support plate as its input.

It calculates the response of the fuel assemblies in a row up to the maximum number of fuel assemblies in a row loaded in the core. Figure 3.1-1 shows a cross section of the core and the response of up to 17 fuel assemblies in a row is calculated when they are accelerated in the direction parallel to the row.

The analysis model of multiple fuel assemblies in the FINDS code is shown in Figure 3.1-2. The fuel assemblies are located in the space surrounded by rigid walls (the neutron reflector on both sides and the upper core plate and lower core support plate at the top and bottom). The space is filled with water. Inside this space, the fuel assemblies vibrate and impact with each other or with the neutron reflector in the case of an earthquake with large acceleration. Considering these interactions, the fuel assemblies' horizontal displacement and the impact force generated at the grid spacer location are calculated.

The units used in the FINDS code are seconds (time), mm (length), kgf (force) and kgf·mm (work, energy). The same units are used in this report.

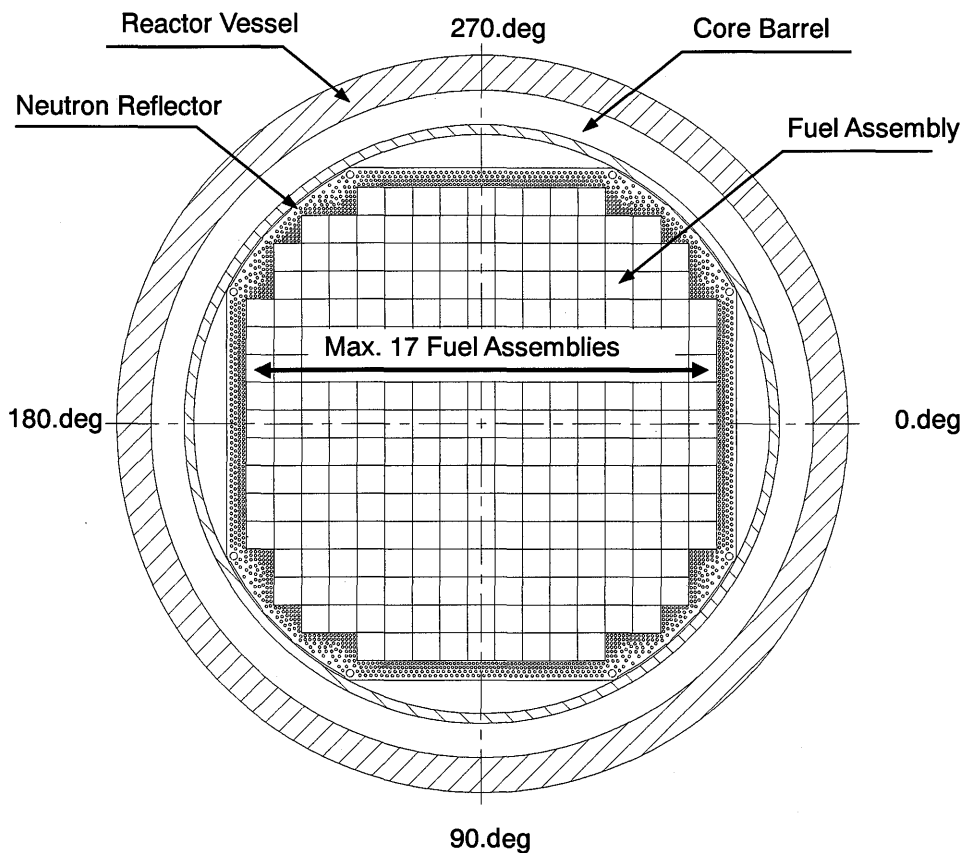


Figure 3.1-1 Cross Section of the US-APWR Core

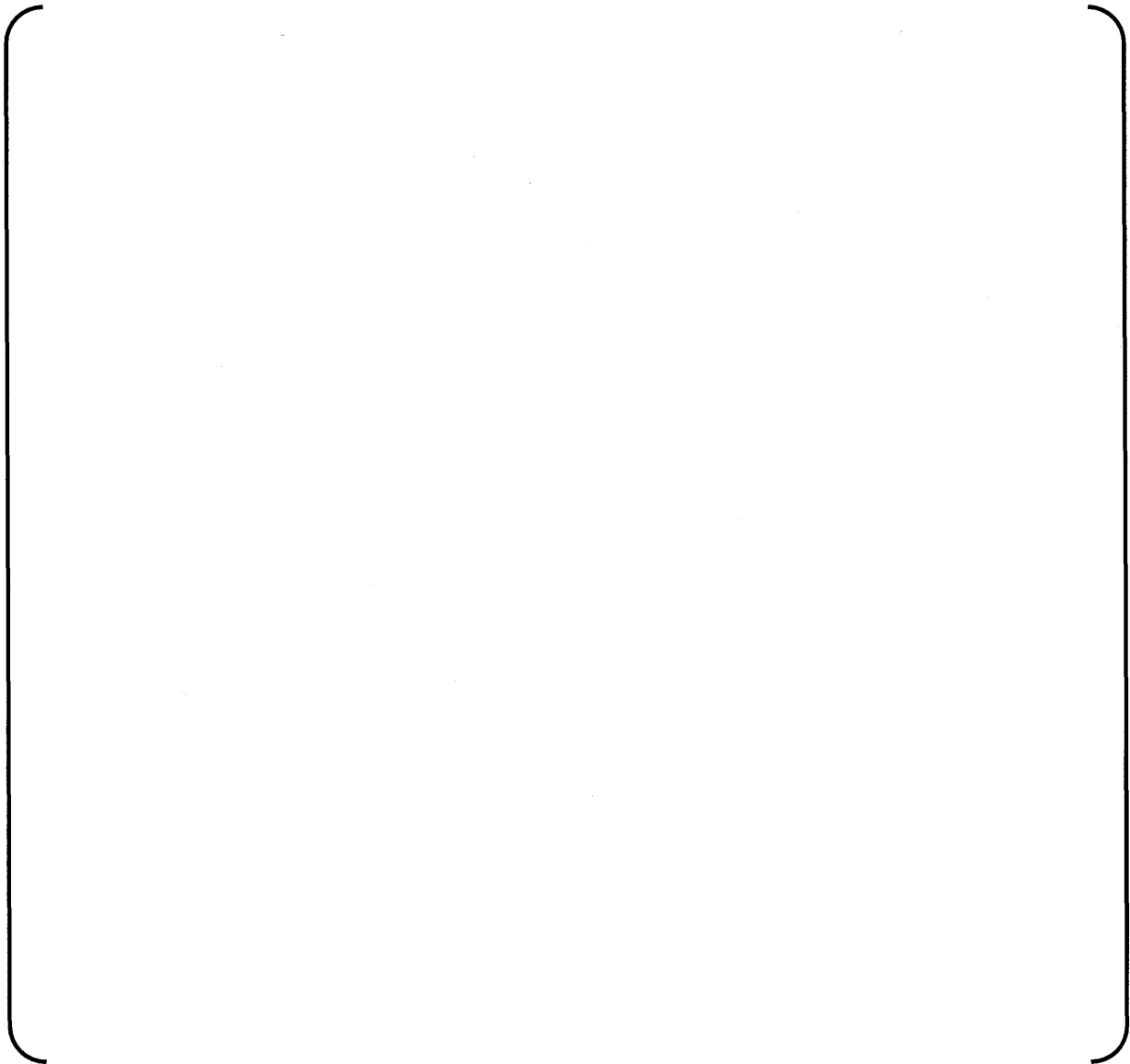


Figure 3.1-2 Model for Lateral Impacting of US-APWR Fuel Assemblies Model

3.2 Detailed Model of Fuel Assemblies in the FINDS Code

Details of the fuel assembly model in the FINDS code are shown in Figure 3.2-1. The model is basically made from FEM beam elements and the following detailed modeling is introduced to simulate fuel assemblies' vibration behavior with interactive collisions.

(1) Beam element

A grid spacer interval called the "span" is divided into { } elements. The mass matrix of the beam is generated using the span length and mass of the fuel assembly per unit length . The resulting equivalent stiffness matrix is based on the moment of inertia and Young' modulus of the fuel rods and the control rod guide thimbles in the fuel assembly.

(2) { }

To simulate the support at the upper and lower nozzle by the fuel assembly guide pins on the core plates, { } are used at the ends of the fuel assembly beam model to restrain {

{ }

(3) { }

At the nodes corresponding to grid spacer locations, { } are used to

{ }

(4) Impact model at grid spacer location

There is elastic impact behavior when the fuel assemblies collide with each other or with the neutron reflector at grid spacer elevations. In addition, in-elastic impact occurs when there is sliding of the fuel rod relative to the grid spacer or the impact force exceeds the elastic limit of the grid spacer. Special models at the grid spacer location are used to simulate these complicated interactions, with the details described in Section 3.7. {

{ }

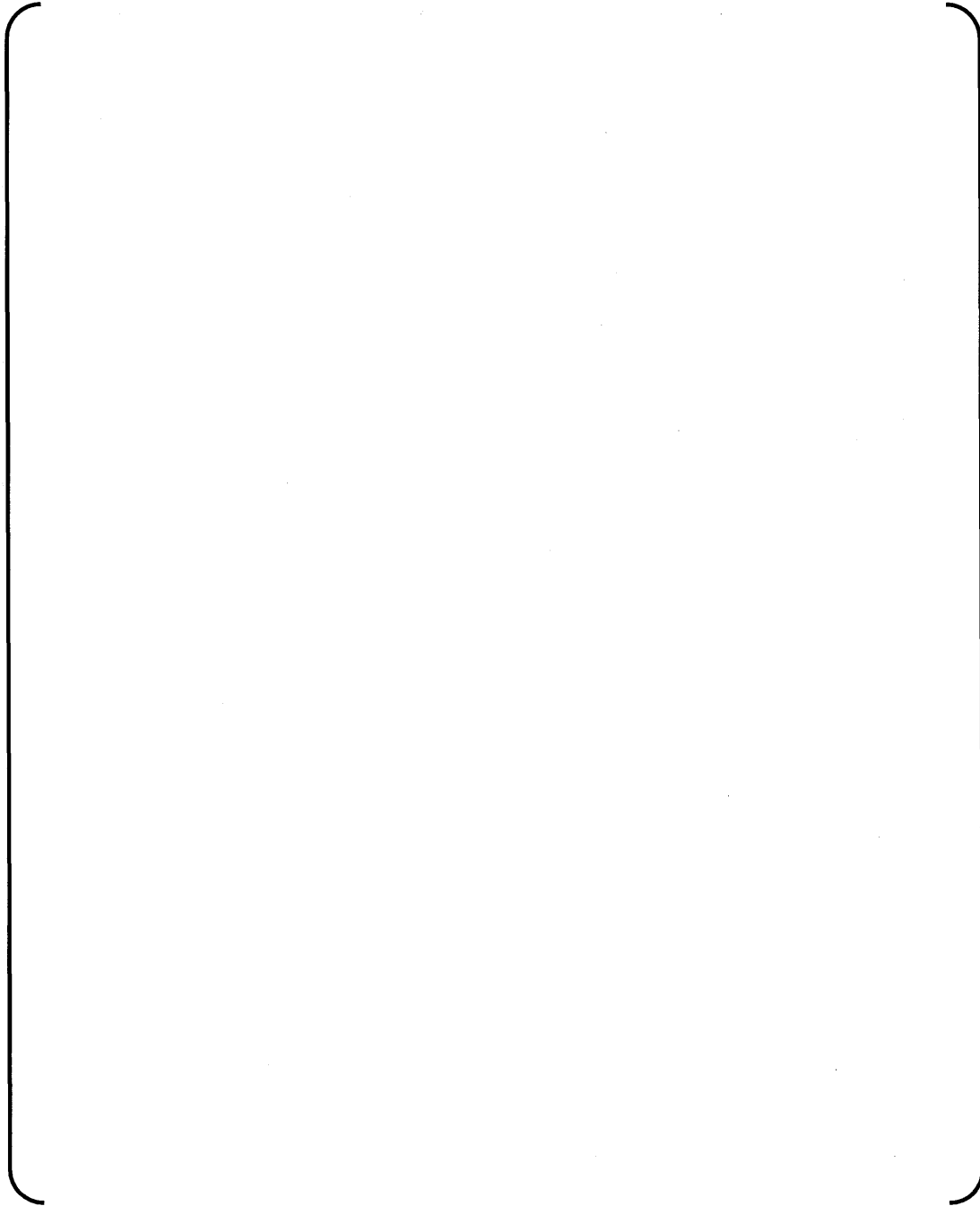


Figure 3.2-1 Vibration Model for the US-APWR Fuel Assembly

3.3 Fundamental Equation for Vibration of the Fuel Assembly

In order to describe the motion of the fuel assembly, the assembly is treated as a single beam (), as previously illustrated in the Figure 3.2-1.

The fuel assembly is modeled with two-dimensional beam elements with n nodes. Each node has two degrees of freedom corresponding to transverse and rotational displacements.

In Equation (3.3-1), Y is the absolute displacement of the nodes. The fuel assemblies are supported at their top and bottom ends by the upper core and the lower core support plates and they are vibrated by the acceleration of these plates. The core barrel, with the neutron reflector, and the core plates are rigid structures and move laterally with the lower core support structure. X₀ is as the absolute displacement of the core barrel corresponding to the fuel assembly nodes. Then from the balance between the inertia force and the reaction force due to the deflection of the fuel assembly gives the following equation.

$$-M\ddot{Y} = K(Y - X_0) \quad \dots \quad (3.3-1)$$

Setting the relative displacement to core barrel of fuel assembly X=Y-X₀,

$$M\ddot{X} + KX = -M\ddot{X}_0 \quad \dots \quad (3.3-2)$$

The fluid damping is proportional to relative velocity \dot{X}_0 since the displacement of coolant moving with the core barrel is equal to that of the core barrel, and the structural damping is also proportional to \dot{X}_0 . Adding the effect of damping to the above equation, and setting the external force F_R as the force due to the impact of the fuel assemblies, the vibration equation is as follows.

$$M\ddot{X} + C\dot{X} + KX = -M\ddot{X}_0 + F_R \quad \dots \quad (3.3-3)$$

where

n: Number of nodes

$$X = (x_1 \ \theta_1 \ x_2 \ \dots \ \theta_{n-1} \ x_n \ \theta_n)^T$$

: Nodal displacements of the fuel assembly beam relative to barrel

$$\ddot{X}_0 = (\ddot{x}_{01} \ \ddot{\theta}_{01} \ \ddot{x}_{02} \ \dots \ \ddot{\theta}_{0n-1} \ \ddot{x}_{0n} \ \ddot{\theta}_{0n})^T$$

: Seismic acceleration of core barrel by absolute coordinate

M, C, K

: Mass, damping and stiffness matrices of the fuel assembly beam (2n x 2n)

Grouping and re-ordering components in the matrices by free and fixed displacement components,

$$\begin{bmatrix} M_{ff} & M_{fs} \\ M_{sf} & M_{ss} \end{bmatrix} \begin{Bmatrix} \ddot{X}_f \\ \ddot{X}_s \end{Bmatrix} + \begin{bmatrix} C_{ff} & C_{fs} \\ C_{sf} & C_{ss} \end{bmatrix} \begin{Bmatrix} \dot{X}_f \\ \dot{X}_s \end{Bmatrix} + \begin{bmatrix} K_{ff} & K_{fs} \\ K_{sf} & K_{ss} \end{bmatrix} \begin{Bmatrix} X_f \\ X_s \end{Bmatrix} = - \begin{bmatrix} M_{ff} & M_{fs} \\ M_{sf} & M_{ss} \end{bmatrix} \begin{Bmatrix} \ddot{X}_{0f} \\ \ddot{X}_{0s} \end{Bmatrix} + \begin{Bmatrix} F_{Rf} \\ F_{Rs} \end{Bmatrix}$$

.... (3.3-4)

where

Suffix f: Component for free nodes

Suffix s: Component for supported nodes

$$X_f = (\theta_1 \quad x_2 \quad \theta_2 \quad \dots \quad x_{n-1} \quad \theta_{n-1} \quad \theta_n)^T :$$

Nodal displacement vector of free components

$$X_s = (x_1 \quad x_n)^T = (0 \quad 0)^T : \text{Nodal displacement at support points}$$

Then the equation to be solved is,

$$M_{ff} \ddot{X}_f + C_{ff} \dot{X}_f + K_{ff} X_f = -M_{ff} \ddot{X}_{0f} - M_{fs} \ddot{X}_{0s} + F_{Rf} \quad \dots (3.3-5)$$

For the reaction force at the top and the bottom supports, using the displacement, velocity and acceleration solution,

$$F_{Rs} = M_{sf} (\ddot{X}_f + \ddot{X}_{0f}) + M_{ss} \ddot{X}_{0s} + C_{sf} \dot{X}_f + K_{sf} X_f \quad \dots (3.3-6)$$

Equation (3.3-5) can be rewritten as ;

$$M\ddot{X} + C\dot{X} + KX = P + F_R \quad \dots (3.3-7)$$

where

$$X = (\theta_1 \quad x_2 \quad \theta_2 \quad \dots \quad x_{n-1} \quad \theta_{n-1} \quad \theta_n)^T$$

M, C, K : Mass, damping and stiffness matrices of the fuel assembly beam (2N x 2N), N=n-2

$P = -M\ddot{X}_{0f} - M_{fs}\ddot{X}_{0s}$: Seismic Excitation Force Vector

F_R : Impact force vector

The colliding vibration of one array of the fuel assemblies can be handled by the simultaneous equations, Equation (3.3-7) which are coupled by the impact force vector F_R .

3.4 Mode-superposition Method

Actually the mode-superposing method is used to solve the Equation (3.3-7). It is assumed that the displacement, X can be expressed by the superposition of natural vibration modes as next form.

$$\{X\} = [\bar{A}] \{U\} \quad \dots \quad (3.4-1)$$

where

$$\{U\} = \{u_1, u_2, \dots, u_m\}^T : \text{Modal amplitude}$$

$$[\bar{A}] = [A] [B]$$

$$[A] = (\{A\}_1, \{A\}_2, \dots, \{A\}_m)$$

$$\{A\}_i : \text{Normalized i-th mode shape}$$

[B] : m x m diagonal matrix whose i-th element b_i can be determined from the orthogonal relation between vector [A] and matrix [M],

$$b_i = 1 / \sqrt{\{A\}_i^T [M] \{A\}_i}$$

m: Maximum mode number ($m \leq 2n-2$)

Then assuming no interaction of damping between any two different modes, Equation (3.4-1) is expressed as Equation (3.4-2):

$$\{\ddot{U}\} + 2[O] [H] \{\dot{U}\} + [O]^2 \{U\} = \{G(t)\} \quad \dots \quad (3.4-2)$$

where

[O]: Natural angular frequency matrix, m x m diagonal

[H]: Damping factor (fraction of critical damping) matrix, m x m diagonal

$$\{G(t)\} = [\bar{A}]^T (\{P\} + \{F_R\})$$

3.5 Non-linear Damping and Frequency Model

There are strong amplitude-dependencies especially for the 1st mode vibrational damping and frequency in the case of a PWR fuel assembly. These characteristics are caused by the contact mechanism between fuel rods and grid spacers as shown in Figure 3.5-1. As the fuel rods are axially supported only by the friction interaction with the grid spacers, the axial and lateral slippage and/or the lift-off of fuel rods from the supporting grid spacer springs and dimples becomes significant as the deflection of the fuel assembly increases. Then a hysteresis-type load-deflection curve for the fuel assembly, which is determined from lateral loading tests of the fuel assembly, as shown in Figure 3.5-2 is experimentally obtained. The energy loss during a vibrational cycle causes the damping variation and the softening of the stiffness at large deflection causes a decrease in the natural frequency.

For a given time interval, the natural frequency and the critical damping ratio are given by the expression below and shown as the function of the peak-averaged amplitude in Figure 3.5-3.

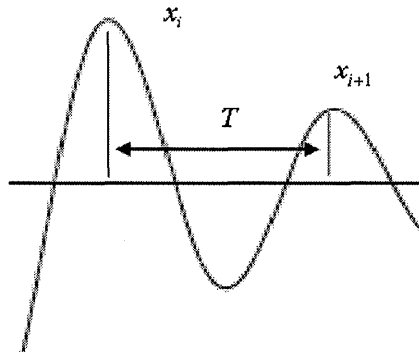
Per the schematic figure of vibration below, for a given time interval, the natural frequency and critical damping ratio are defined by the following expressions.

$$\bar{x} = (x_i + x_{i+1})/2 : \text{Peak - averaged amplitude}$$

$$f = 1/T : \text{Frequency}$$

$$\zeta = 1/\sqrt{1 + (2\pi/\delta)^2} : \text{Damping ratio}$$

$$\delta = \ln(x_i/x_{i+1}) : \text{Logarithmic damping ratio}$$



Using the above expressions, the amplitude dependence of the frequency and damping ratio, (obtained from free vibration tests of the fuel assembly) is shown in Figure 3.5-3.

In order to take into account the non-linear vibrational characteristics of the fuel assembly, the amplitude-dependent viscous damping and frequency model is used in the process to solve the vibrational equation.

In the integration of the equation, the damping factor and natural frequency should be evaluated at every time step for each modal amplitude. Then the Equation (3.4-2) is rewritten as Equation (3.5-1), in which time-dependent matrices [O(t)] and [H(t)] are used. This equation

can be numerically integrated by the feedback of the solution (amplitude) to determine the above matrices.

$$\{\ddot{U}\} + 2[O(t)][H(t)]\{\dot{U}\} + [O(t)]\{U\} = \{G(t)\} \quad \dots \quad (3.5-1)$$

$$\Omega_i = \Omega_i(u(t)) = \Omega_i(t)$$

$$H_i = H_i(u(t)) = H_i(t)$$

Ω_i, H_i : i-th diagonal element of instantaneous matrices, $[\Omega(t)][H(t)]$

Since the experimental damping factors and natural frequencies are correlated with respect to the peak amplitude of vibration, as shown in Figure 3.5-3 for the Mitsubishi conventional 17x17 fuel assembly with a 12ft active length, both parameters in the calculation have to be treated with respect to the instantaneous amplitude. Accordingly, in the simulation analysis $\Omega(u)$ and $H(u)$ should be semi-empirically determined. In the FINDS code, [] .

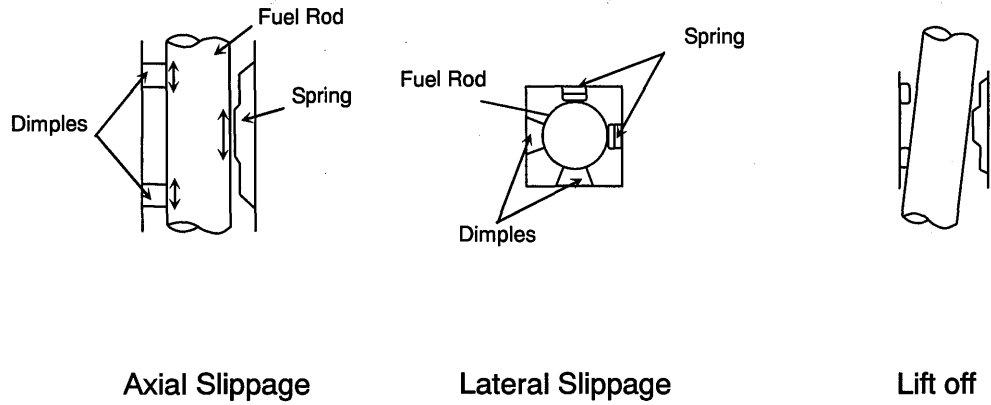


Figure 3.5-1 Non-linear Mechanisms in a Fuel Assembly Structure

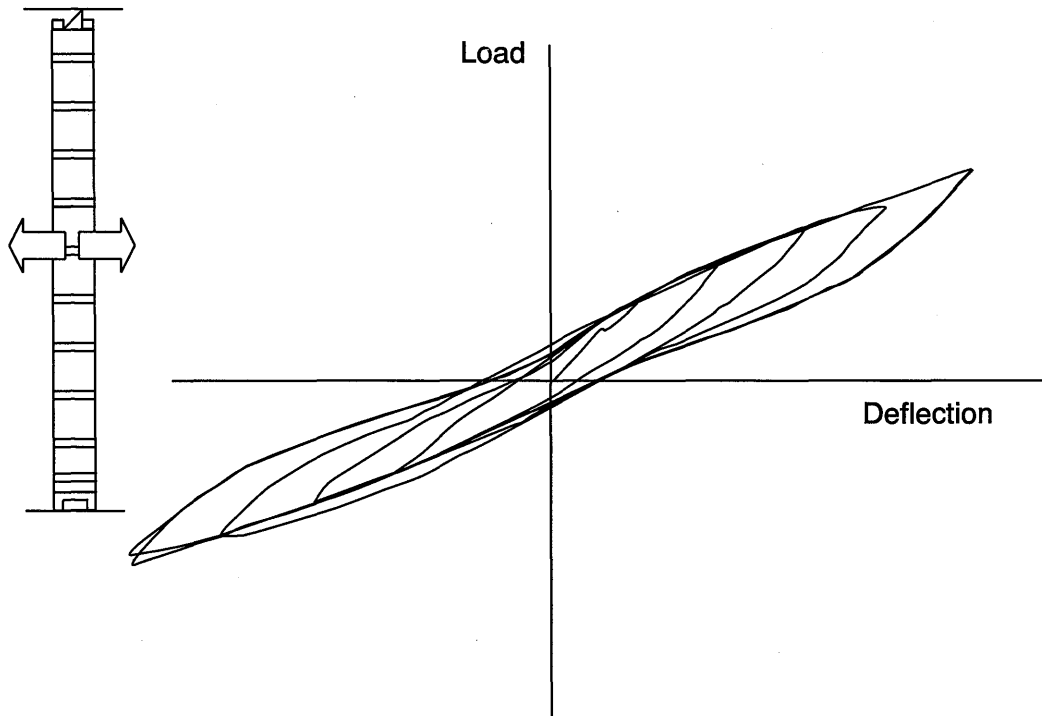


Figure 3.5-2 Load-Deflection Characteristics of a Fuel Assembly due to Lateral Loading

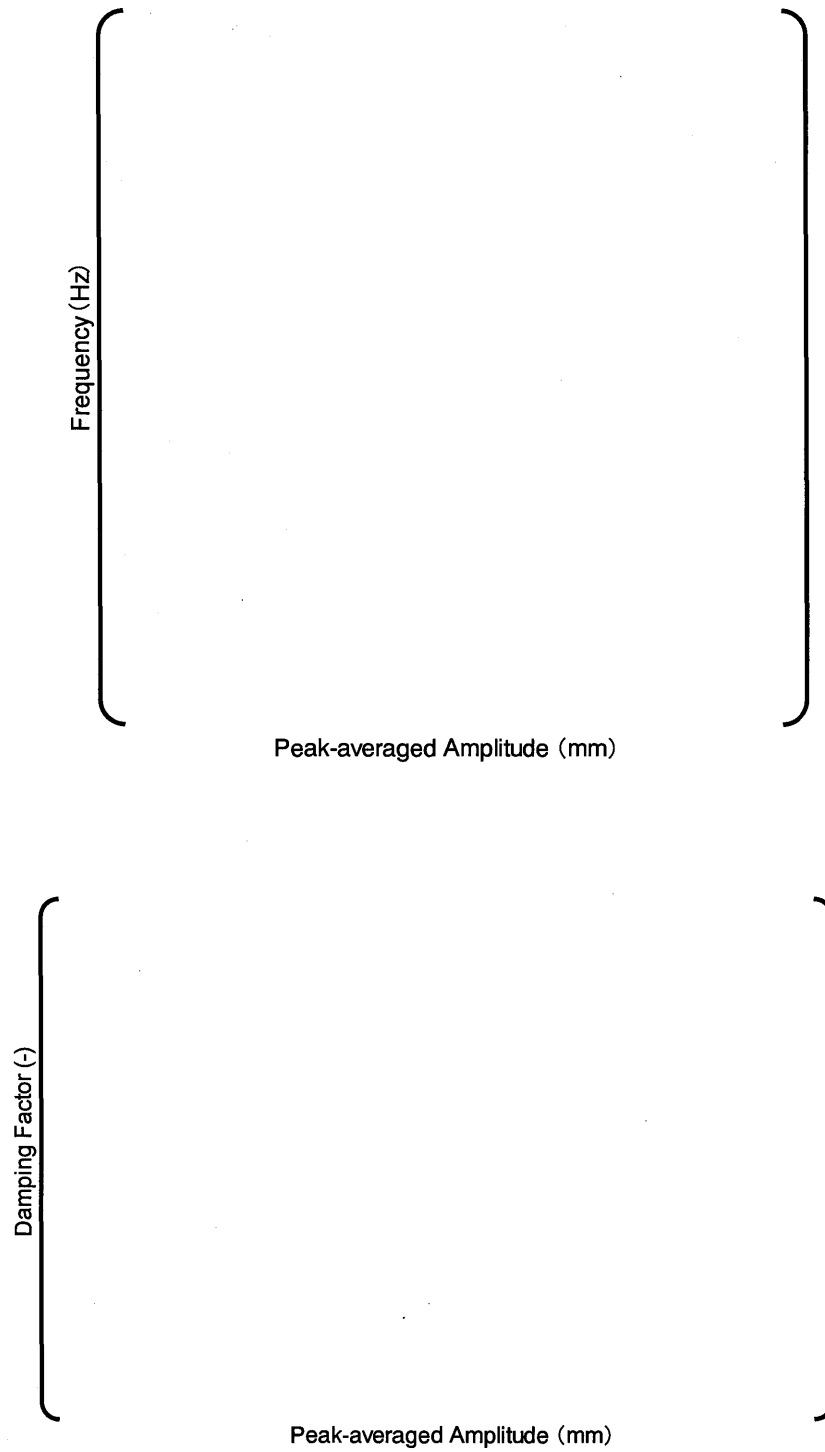


Figure 3.5-3 Amplitude-dependent Frequency and Damping Characteristics of 1st mode

3.6 Solution Process for Non-linear Vibration

The modal equation to be solved for i-th mode can be expressed as follows.

$$\ddot{u} + 2\Omega H\dot{u} + \Omega^2 u = G(t) \quad \dots (3.6-1)$$

where

$u = u_i$: The i-th modal amplitude

$\Omega = \omega_i, H = H_i$: Natural frequency and damping factor for the i-th mode

$G(t) = G_i(t)$: The i-th mode component of external force vector

There is a strong amplitude dependence of the frequency and damping for the 1st mode vibration of a fuel assembly, as described below. These can be modeled by the time-dependent characteristics. A special treatment is thus adopted to solve the 1st mode equation as follows.

$$\Omega = \Omega(t), H = H(t)$$

$$S(t) = \Omega(t)H(t)$$

The natural frequency and damping are treated as constant for the higher order vibration modes.

$$S(t) = S = const.$$

In order to solve the Equation (3.6-1) accounting for the amplitude dependence, it is assumed that,

$$u = \left[\quad \right] \quad \dots (3.6-2)$$

so that \dot{u} and \ddot{u} are

$$\dot{u} = \left[\quad \right] \quad \dots (3.6-3)$$

$$\ddot{u} = \left[\quad \right] \quad \dots (3.6-4)$$

Substituting equations from (3.6-2) to (3.6-4) into equation (3.6-1) gives:

$$\left[\quad \right] \quad \dots (3.6-5)$$

or

$$\left[\quad \right] \quad \dots (3.6-6)$$

where

$$\left[\begin{array}{c} \dots \\ \dots \end{array} \right] \dots \quad (3.6-7)$$

For a small increment h in a given time step, t , using the Taylor's expansion for y gives:

$$y(t+h) = y(t) + h\dot{y}(t) + \frac{h^2}{2}\ddot{y}(t) + \dots$$

$$y(t-h) = y(t) - h\dot{y}(t) + \frac{h^2}{2}\ddot{y}(t) + \dots$$

Summing these two equations and neglecting the third order and higher terms gives:

$$y(t+h) + y(t-h) = 2y(t) + h^2\ddot{y}(t) \quad \dots \quad (3.6-8)$$

Substituting the Equation (3.6-6) into the Equation (3.6-8) gives:

$$y(t+h) = -y(t-h) + \left[\begin{array}{c} \dots \\ \dots \end{array} \right] \dots \quad (3.6-9)$$

An alternate expression for equation (3.6-9) is,

$$y_{n+1} = \left[\begin{array}{c} \dots \\ \dots \end{array} \right] \dots \quad (3.6-10)$$

where

$$\left[\begin{array}{c} \dots \\ \dots \end{array} \right] \dots \quad (3.6-11)$$

$n-1, n, n+1$: sequential time steps

Equation (3.6-11) can be sequentially solved when y_0 and y_1 are provided as initial values.

The displacement, x is then obtained from y using Equations (3.4-1) and (3.6-2),

$$y \rightarrow u \rightarrow x$$

The flow diagram of the above calculation is shown in Figure 3.6-1.

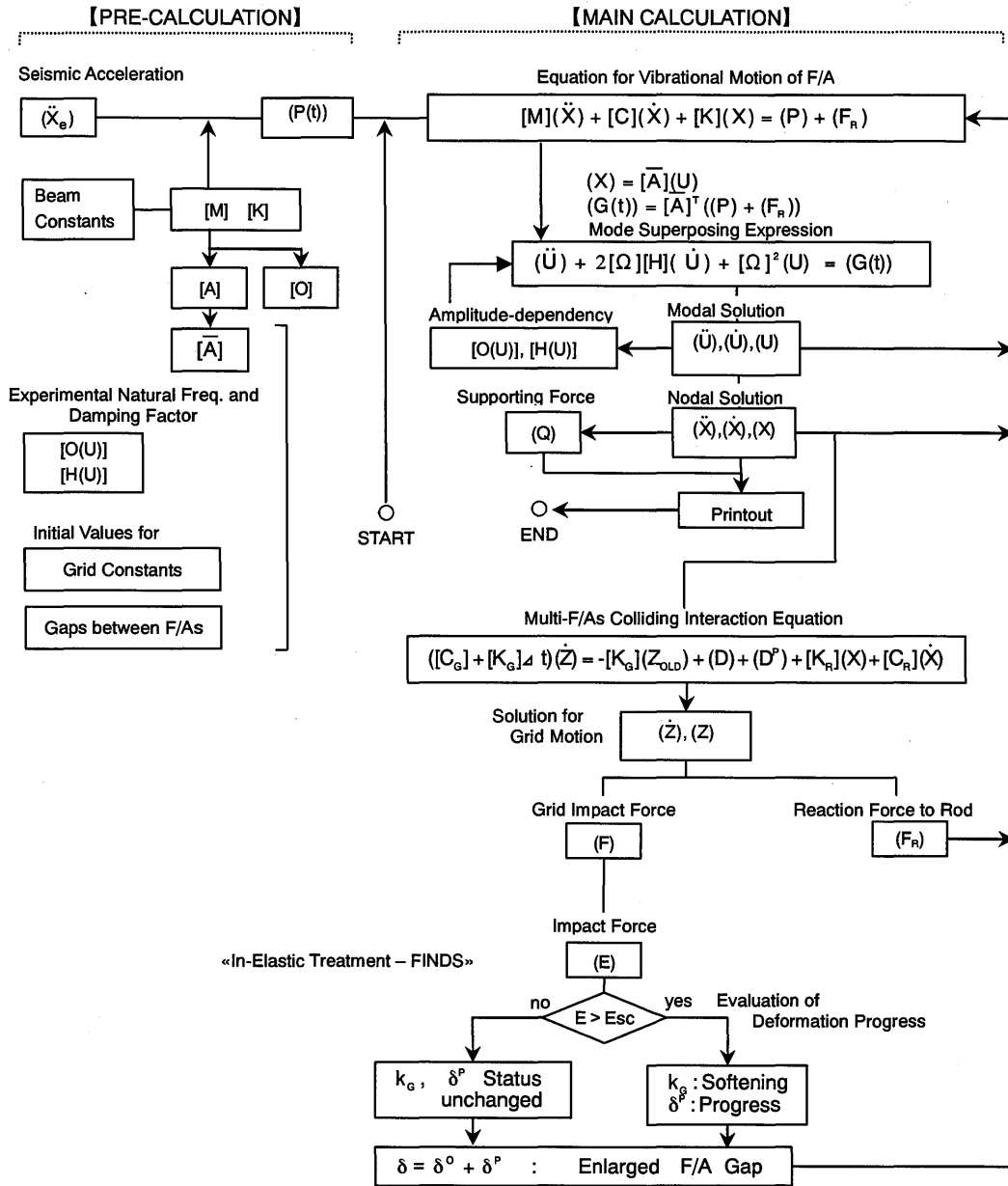


Figure 3.6-1 FINDS Code Basic Flow Diagram

3.7 In-elastic Impact Model

3.7.1 Multi-Fuel Assembly Impact Model

In order to solve the multi-fuel assembly impacting interaction, one transverse array of grid spacers at the same elevation is modeled as shown in Figure 3.7.1-1. One grid spacer is modeled by two pairs of a spring and a damper element located on both sides of the beam and respectively shown as k_g and c_g , because impacting needs to be considered to occur on both sides of the fuel assembly. Gaps that exist between adjacent fuel assemblies are also modeled in the grid spacer models. Another set of a spring and a damper element, which are expressed by k_r and c_r , are connected to the k_g and c_g elements. The formulation of this system of equations is described in detail in the following subsection.

Considering the equilibrium of forces at node j , shown in the Figure 3.7.1-1, the next relationship is obtained.

$$f_j - f_{j+1} - f_{r_j} = 0 \quad \dots \quad (3.7-1)$$

where

$$f_j = (z_{j-1} - z_j - d_j^0 - d_j^P) k_{g_j} + (\dot{z}_{j-1} - \dot{z}_j - \dot{d}_j^0 - \dot{d}_j^P) c_{g_j}$$

f_{j+1} : similar as above

$$f_{r_j} = (z_j - x_j) k_{r_j} + (\dot{z}_j - \dot{x}_j) c_{r_j}$$

z_j : displacement of grid spacer at joint j

x_j : displacement of rods at joint j

d_j^0 : initial gap between adjacent fuel assemblies (j -th gap),

d_j^P : plastic deformation of the j -th gap spring element

Using Equation (3.7-1), the equation for the multi-fuel assembly interaction at a given grid spacer elevation is obtained as follows.

$$([C_G] + [K_G] \Delta t) \{\dot{z}\} = -[K_G] \{Z_{OLD}\} + \{D\} + \{D^P\} + [K_R] \{X\} + [C_R] \{\dot{X}\} \quad \dots \quad (3.7-2)$$

where

Since the right hand of Equation (3.7-2) is known, $\{\dot{Z}\}$ can be theoretically solved. Then $\{Z_{NEW}\}$ is obtained by the Equation (3.7-3). However, the spring and damping constants need to be determined consistent while being consistent with the boundary condition for $\{Z\}$. Therefore, the Equations (3.7-2) and (3.7-3) should be solved by the iterative convergent calculation method. Now that $\{\dot{Z}\}$ and $\{Z_{NEW}\}$ have been solved, the grid spacer impact forces f_j , f_{j+1} and the reaction force to the rods f_{rj} can be determined. By applying the above process for every grid spacer elevation of the fuel assemblies, we can complete the combined interaction calculation for one array of fuel assemblies.

When the impact occurs at the j-th gap, the elastic energy absorbed in the grid spacer (j-th gap spring) can be calculated as follows.

$$E_j = \int f_j d\delta_j^E$$

where

$$\delta_j^E = Z_{j-1} - Z_j - \delta_j^0 - \delta_j^P \quad (Z_0 = Z_{N+1} = 0)$$

δ_j^0 : Initial gap at j-th gap

δ_j^P : Gap change at j-th gap due to plastic deformation

By comparing the E_j with the ESC_j which is experimentally derived as explained in the next subsection, the current status for the stiffness (k_{gj}) and the plastic deformation (δ_j^P) is determined as follows.

	Deformation δ_j^P	Stiffness k_{gj}	ESC_j
$E_j > ESC_j$	Progress	Softening	Update (= E_j)
$E_j \leq ESC_j$	No progress	Unchanged	Unchanged

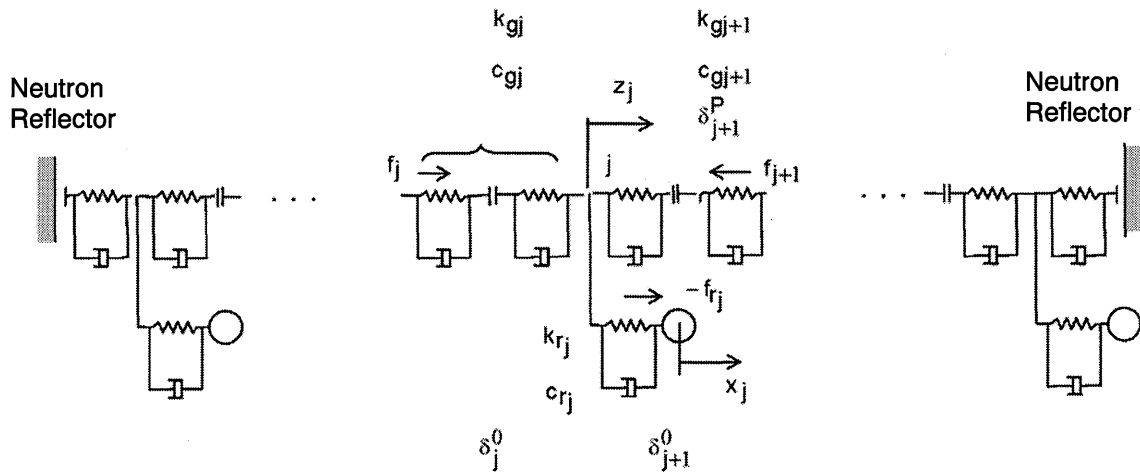


Figure 3.7.1-1 Multi-Fuel Assembly Impact Model

3.7.2 Stiffness and Viscous Damping Coefficient in the Impact Model

The two types of stiffness (k_g and k_r) and viscous damping coefficients (c_g and c_r) are used in impact model as shown in Figure 3.7.1-1. These constants are defined as follows.

(1) Stiffness

Figure 3.7.2-1(a) shows one grid spacer portion of a fuel assembly. On each side of the grid spacer node, $2k_g$ is used to represent the stiffness of a half-sized grid spacer. The value of k_g represents the stiffness of whole grid spacer, which is illustrated in Figure 3.7.2-1(b), and can be experimentally obtained from the grid spacer impact test shown in Figure 3.7.2-2. The stiffness k_r connects the fuel rod with the grid spacer. Grid spacer springs and dimples, both parallel and tangential to the direction of impact, contribute to this stiffness. Since the slip between the fuel rod and dimple or spring in the tangential direction affects the stiffness k_r , it cannot be directly determined. {

impact test.

(2) Viscous damping

The damping factor c_g and c_r also can not be directly determined either. They are set based on the following process. The grid spacer impact test shown in Figure 3.7.2-2 gives us the information related to the rebound characteristics of grid spacer. Defining the restitution coefficient "e" as the square root of the rebound angle to the initial angle, the value 'e' is approximately { }. When the impact behavior of one grid spacer half on the left side wall is treated as shown in Figure 3.7.2-1(c), the region related impact is re-expressed as in Figure 3.7.2-1(d). Here the mass M is given corresponds to that of one span length of fuel assembly and the combined stiffness K is given as,

$$K = 1 / \left(\frac{1}{2k_g} + \frac{1}{k_r} \right)$$

Assuming that the rebound behavior is similar to that of the grid spacer impact test (the same restitution coefficients "e"), the value of C is determined as follows.

$$e = \exp\left(\frac{\zeta\pi}{\sqrt{1-\zeta^2}}\right) \quad \zeta = C/C_{cr} \quad C_{cr} = 2\sqrt{MK}$$

After 'C' is obtained from above, c_g and c_r are defined as follows.

$$c_g = \frac{2k_g}{K} C \quad c_r = \frac{k_r}{K} C$$

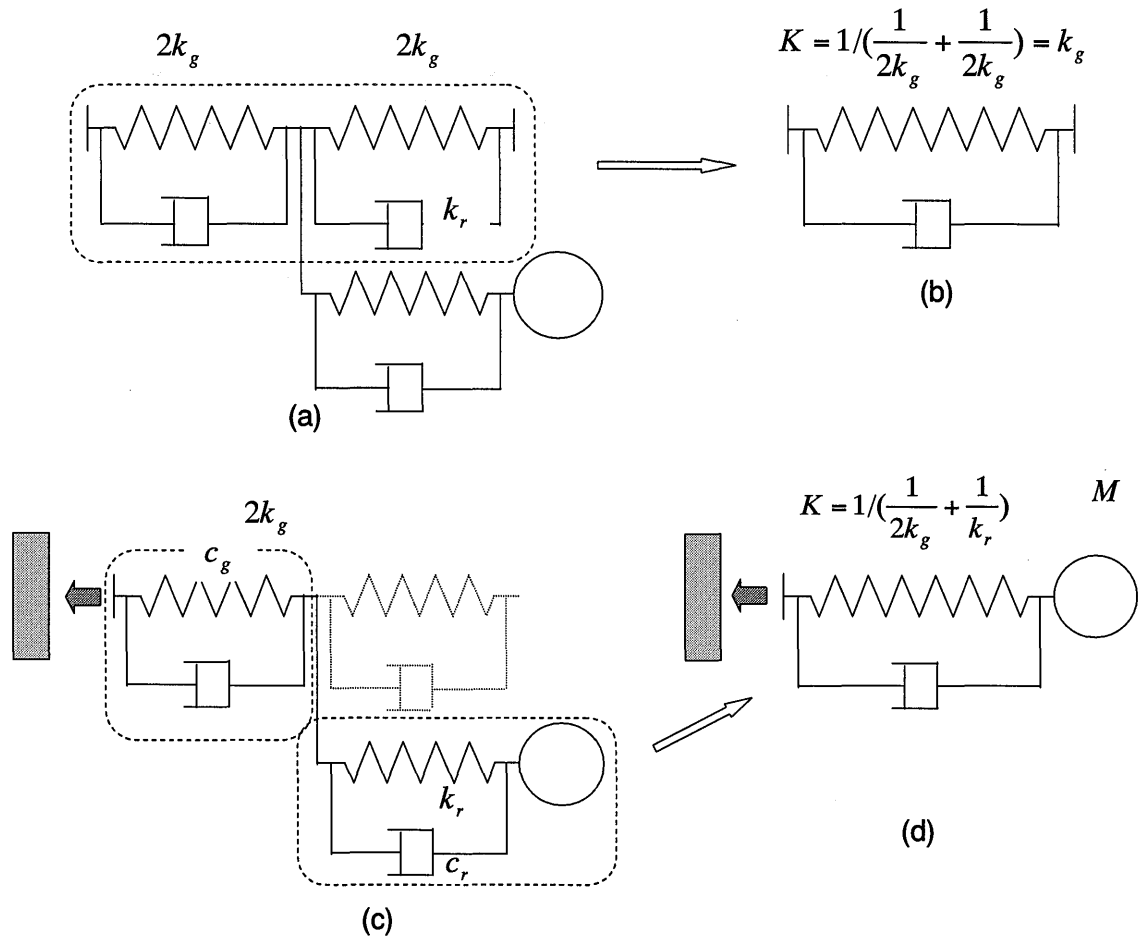


Figure 3.7.2-1 Modeling of Grid Spacer Characteristics

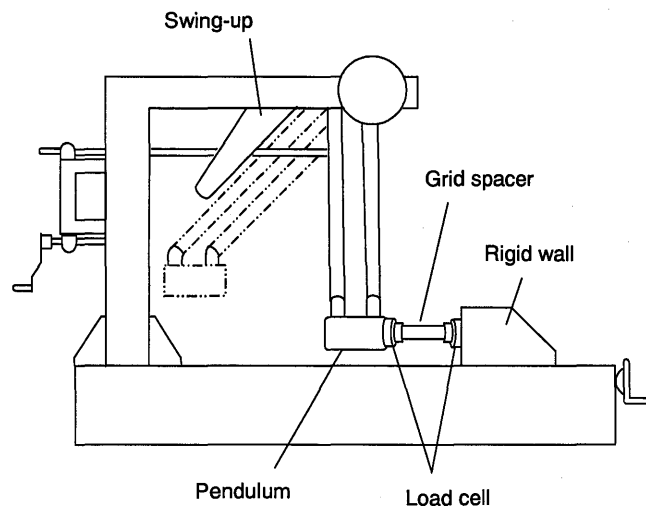


Figure 3.7.2-2 Grid Spacer and Pendulum Type Impact Test

3.7.3 Description of the Grid Spacer Deformation Progression

When the impact force at the grid spacer exceeds its elastic limit, buckling occurs in one row of grid spacer cells. The buckling may propagate to the next row depending on the impact force generated in next impact. As mentioned above, semi-empirical rules are used in the FINDS code to express the grid spacer deformation progress. They are derived from the experimental results obtained by the "pendulum and grid spacer" type impact and deformation tests shown in Figure 3.7.2-2. Figure 3.7.3-1 shows the continuous "load-deflection" curves of the sequential grid spacer impact tests, and the typical "load-deflection" curves of the two consecutive impacts are shown in Figure 3.7.3-3 schematically.

- a) Current plastic deformation of the grid spacer is set as d at point, a in the Figure 3.7.3-2.
- b) The path a - b is the elastic deformation process for the first impact. The impact energy of $E = \int_a^b f d\delta$ is absorbed in the grid spacer structure elastically.
- c) The plastic deformation progresses when the absorbed energy E exceeds E_1 (area a - b - b') which is the elastic limit energy for the current status.
- d) d at point d means the progressed plastic deformation.
- e) E_2 (Area d - c - c'), which experimentally is always bigger than E_1 , is the updated elastic limit energy for the new status after the impact.
- f) The slope of the path c - d shows that the stiffness is reduced by the deformation and the elastic deformation process of the second impact is almost consistent with the path c - d .

The elastic limit energies such as E_1 and the grid spacer stiffness are uniquely correlated with the grid spacer deformation as schematically shown in Figure 3.7.3-3 schematically. With progressive deformation, the stiffness decreases and the elastic limit energy increases. The latter is the most important characteristics because it stops (or controls) the deformation progress: if the impact energy E is less than E_1 , plastic deformation will remain constant. Then this elastic limit energy is named ESC (Energy Storage Capacity).

By using this concept of ESC, it is possible to model the elastic-plastic impact behavior of the grid spacer. In the FINDS code, the following two experimental correlations are used to express the grid spacer deformation progress.

$$\text{Stiffness} \quad ; \quad k_g = g_1(ESC)$$

$$\text{Deformation} \quad ; \quad \delta^P = g_2(ESC)$$

In Figure 3.7.3-1 there are several portions where the slope of the "load-deflection" curve (stiffness) gets steeper although in general it decreases. These effects are accounted for by modifying the above correlations between the stiffness, deformation and ESC based on the experimental data. These characteristics will be explained by simple mechanisms as follows:

- A) First, if a certain transverse array of the grid spacer cells is deformed by an impact, then the same grid spacer cells continue to deform by the consecutive impacts, until the cells shrink so much that the grid spacer straps effectively touch the fuel rods in them, during which the gradual decrease of the stiffness is observed.
- B) However, once the deformation in the array reaches the above limit, then the stiffness is increased by the existence of the fuel rods, and there is no further deformation progress with these cells.
- C) For the following consecutive impacts one of the new array of the grid spacer cells takes part with the further deformation progress following the similar mechanism to A)~B).
- D) With the same or increased pendulum angles, the process to A) ~ C) are repeated in the deformation process in Figure 3.7.3-1.

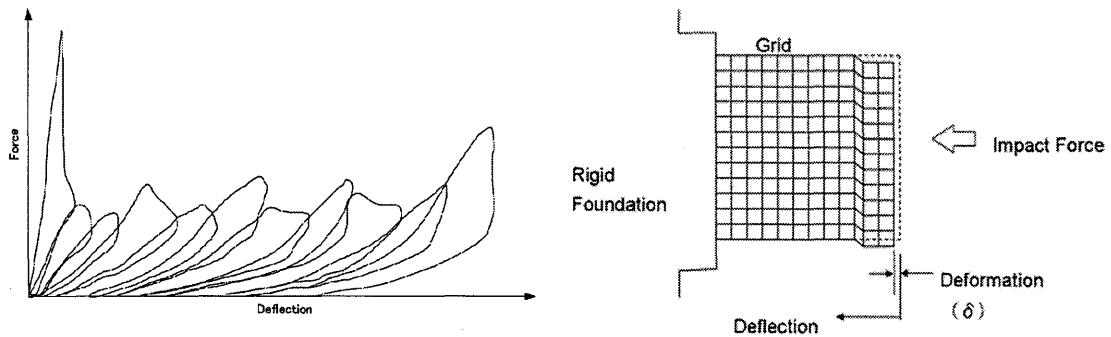


Figure 3.7.3-1 Load-Deflection Curves of Sequential Impacts

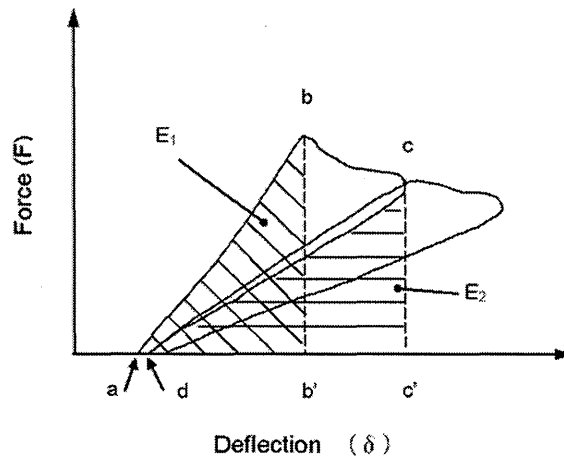


Figure 3.7.3-2 Typical Load-Deflection Curves of Two Consecutive Impacts

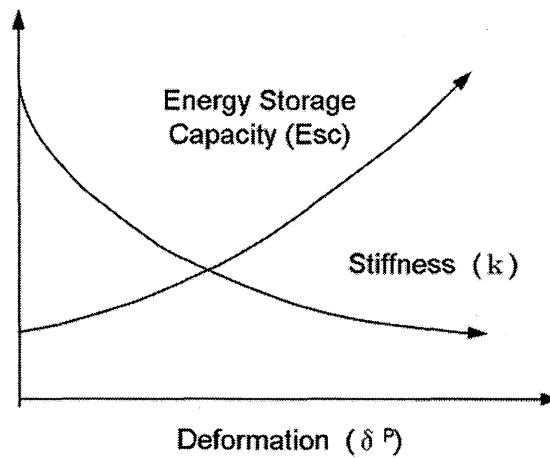


Figure 3.7.3-3 Correlations between ESC, Stiffness and Deformation

4.0 FUNDAMENTAL TESTS FOR MODELING

4.1 Large Amplitude Vibration Test of Fuel Assembly

As shown in Figure 4.1-1, horizontal vibration tests (including lateral pluck tests) have been conducted, using a full scaled mock-up fuel assembly of the conventional 17x17 type with 12ft fuel active length, to semi-empirically adjust the vibrational characteristics in the FINDS code model with special emphasis on the large amplitude characteristics and the effect of water.

[]

[]

In the FINDS code, []

[]

An example is shown in Section A.3.3.5 in Appendix A. []

[]

[]

calculated result is compared with measurements in Figure 4.1-3, [] . The [] has been obtained from the simulation in the same manner as used to evaluate the test results.

[]

[] , is finally determined as shown in Figure 4.1-4. The calculated damping factor as related to peak-averaged amplitude is compared with the measured damping factor in Figure 4.1-5. []

[] . As a result, Figure 4.1-3 is replaced by Figure 4.1-6.

The above treatment is done for the data in air. Using data obtained from the lateral pluck tests in still water, another input data set for the FINDS code is determined. The method is the same as described above. The results are shown in Figure 4.1-7 and 4.1-8. These are obtained by the simulation using [] of the constant damping value . The behavior in water can be simulated without changing $C_f(u)$ and $C_d(u)$.

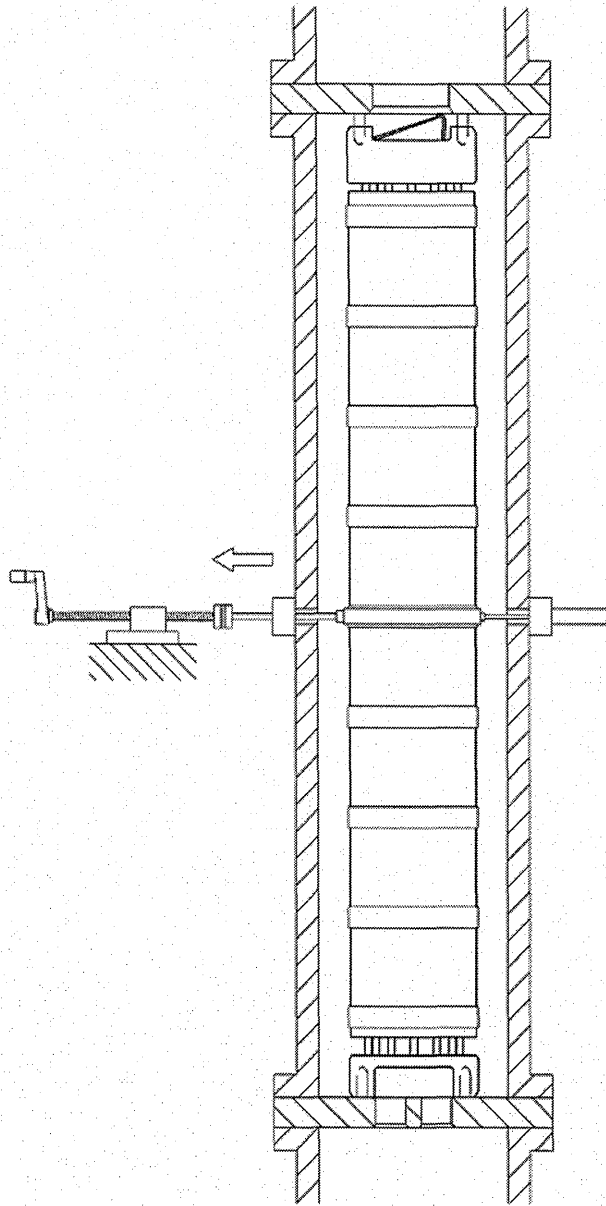


Figure 4.1-1 Fuel Assembly Lateral Pluck Test

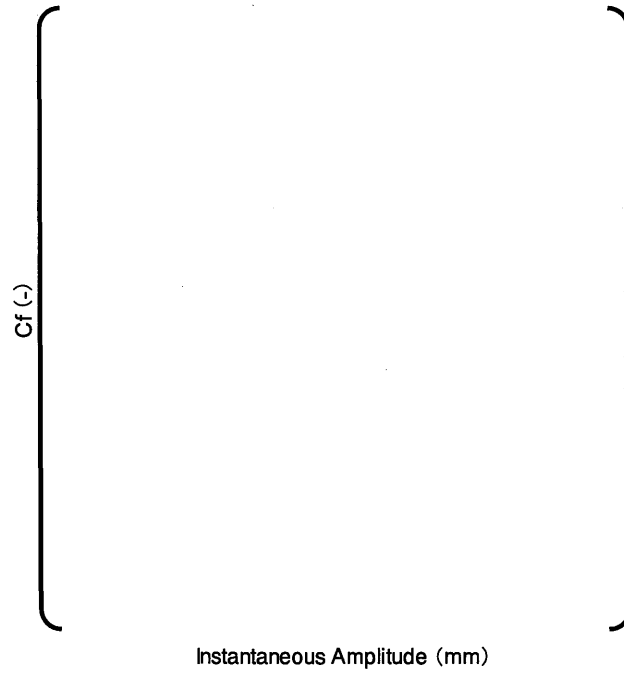


Figure 4.1-2 Amplitude Dependent Coefficients of Natural Frequency in Air

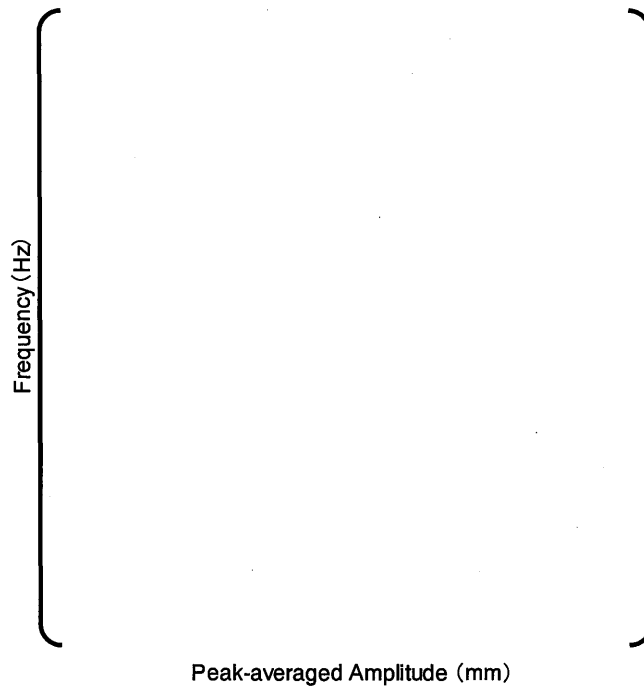


Figure 4.1-3 Amplitude Dependence of Natural Frequency in Air (Assuming Constant Damping)

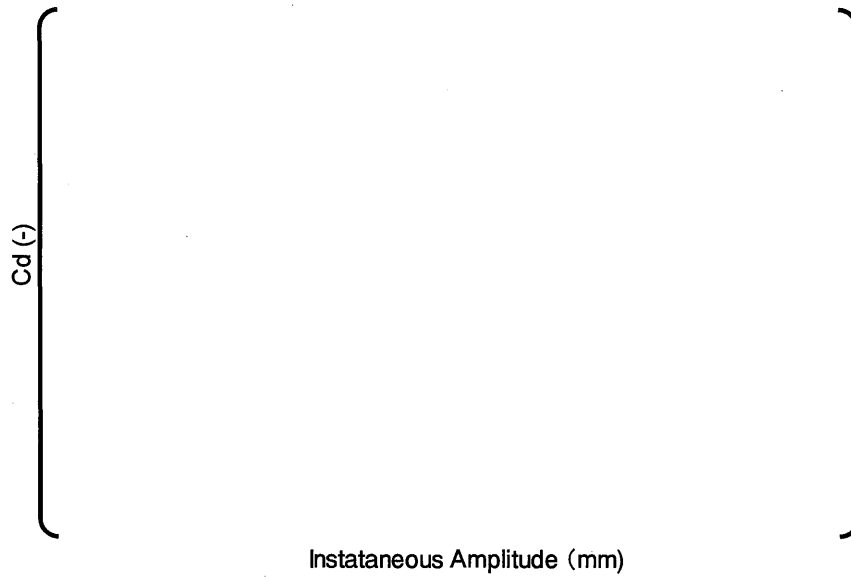


Figure 4.1-4 Amplitude Dependent Coefficients of Damping Factor in Air

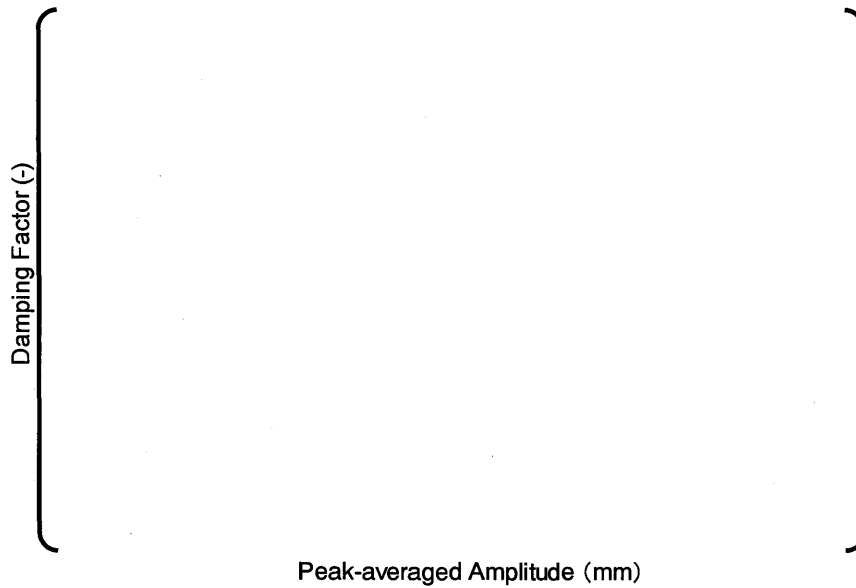


Figure 4.1-5 Amplitude Dependence of Damping Factor in Air

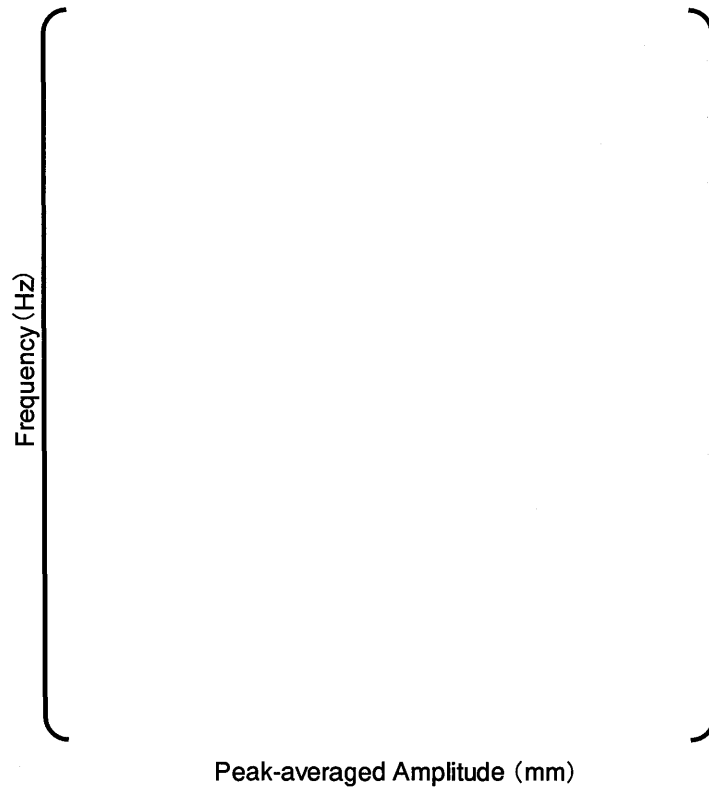


Figure 4.1-6 Amplitude Dependence of Natural Frequency in Air

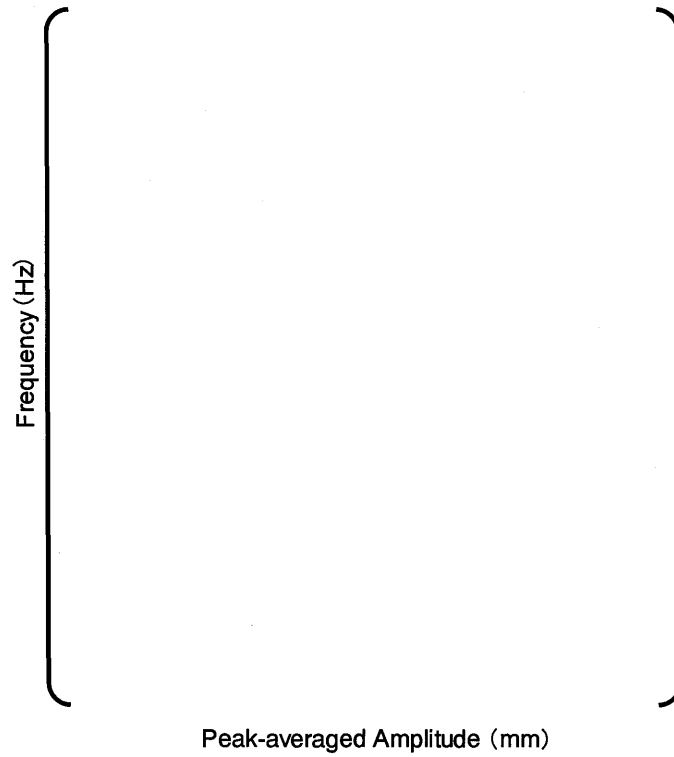


Figure 4.1-7 Amplitude Dependence of Natural Frequency in Still Water

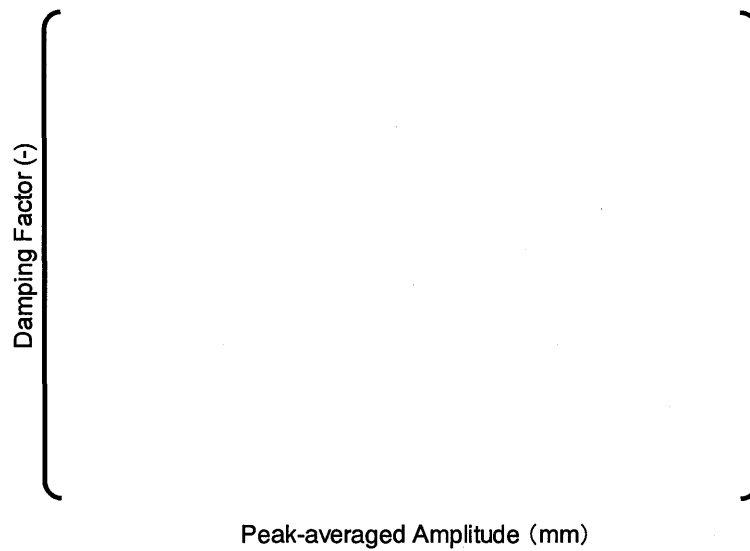


Figure 4.1-8 Amplitude Dependence of Damping Factor in Still Water

4.2 Grid Spacer Impact and Deformation Test

The constants related to the grid spacer deformation progress explained in 3.7.3 are derived by the following process.

4.2.1 Reduction of Characterized Data for the Deformation Progress

From each of the load-deflection curves, relationships between reduced stiffness ratio (RSG) of the grid spacer stiffness, plastic deformation (DP) and ESC are obtained as shown in Figure 4.2.1-1 and 4.2.1-2. These relationships are based on the average values from the impact test results using the several grid spacers.

As seen in Figure 3.7.3-1, the peak value of the load does not necessary decrease but sometimes increases during the repeated impact tests. Figure 4.2.1-3 illustrates a typical example of the load-deflection curve when the peak load increases. In such a case, the local stiffness variations such as kg_1 , kg_2 , kg_3 and deformation energy such as e_1 , e_2 , e_3 defined in the figure, are determined. Then a pair of kg_1 and e_3 values is adopted to generate the relationship between RSG and ESC. The local variation factor $c_i = \left[\quad \right]$ is defined and correlated with the energy e_i . The detailed stiffness variations are then considered to calculate impact energy.

The relationship between 'decrease of stiffness' and 'deformation energy' (RSG = function(ESC), 'plastic deformation and deformation energy') : DP = function(ESC) and the local stiffness variations obtained above are adjusted by the simulation analysis of the impact tests and thus a final model is created.

The analysis results are shown as follows. The angle variation of the pendulum during the test sequence is shown in Figure 4.2.1-5. The angle is started at $\left[\quad \right]$ degrees and increased to a maximum of $\left[\quad \right]$ degrees, while the tests are repeatedly performed. Comparisons of the analysis results to the test results for peak load, plastic deformation and change of restitution coefficient are shown in Figure 4.2.1-6 through Figure 4.2.1-8, respectively. The overlay of the calculated and measured results shows that deformation characteristics are appropriately simulated.

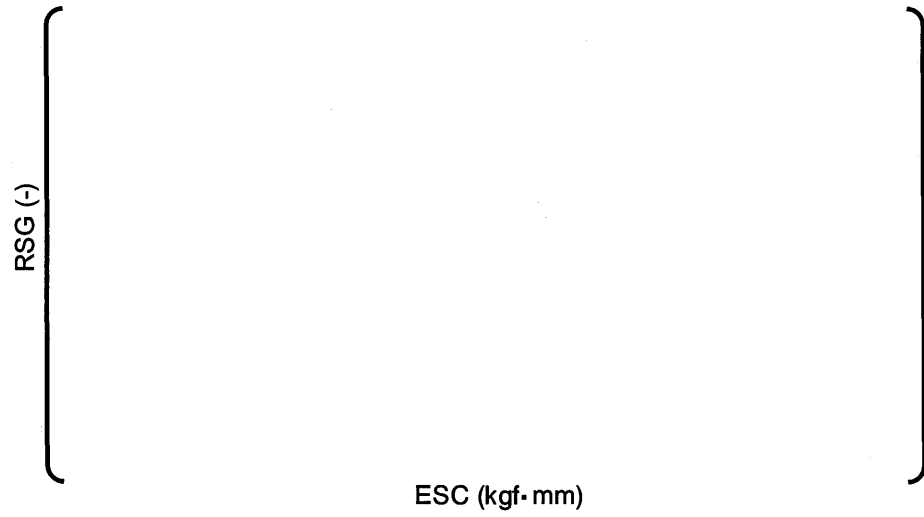


Figure 4.2.1-1 Relationship between Relaxation of Stiffness and ESC

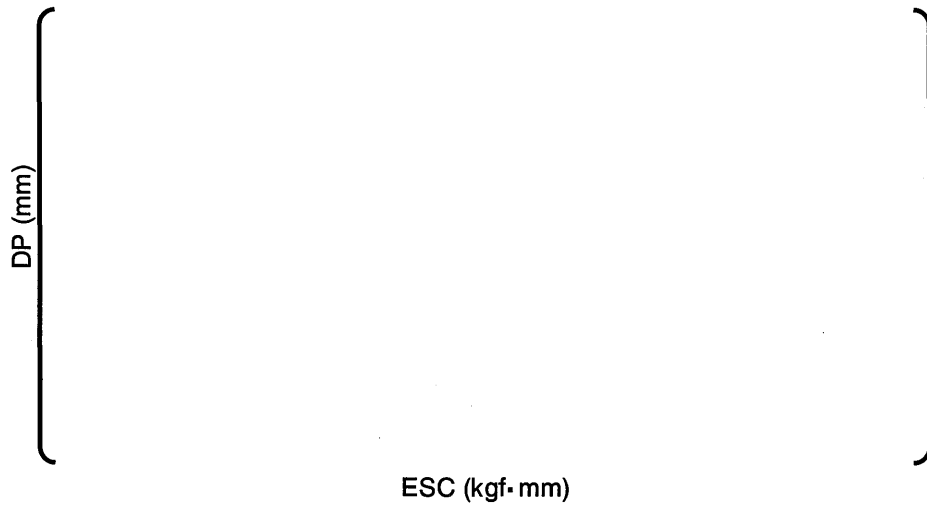


Figure 4.2.1-2 Relationship between Deformation and ESC

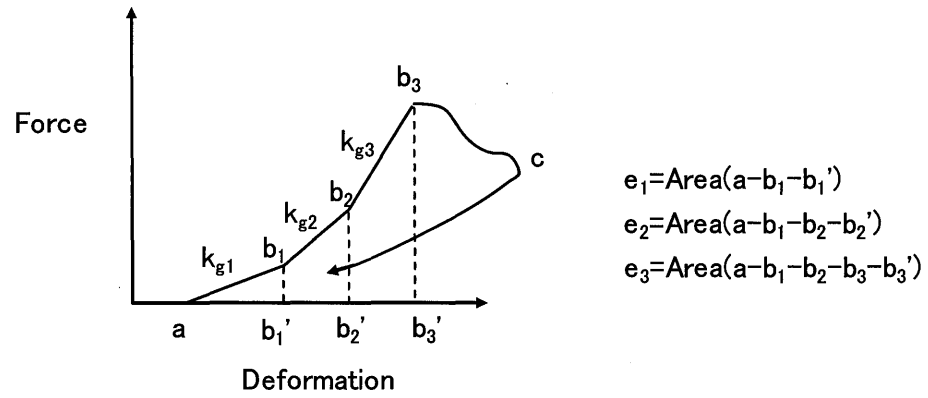


Figure 4.2.1-3 Sampling of Local Stiffness Change and Deformation Energy

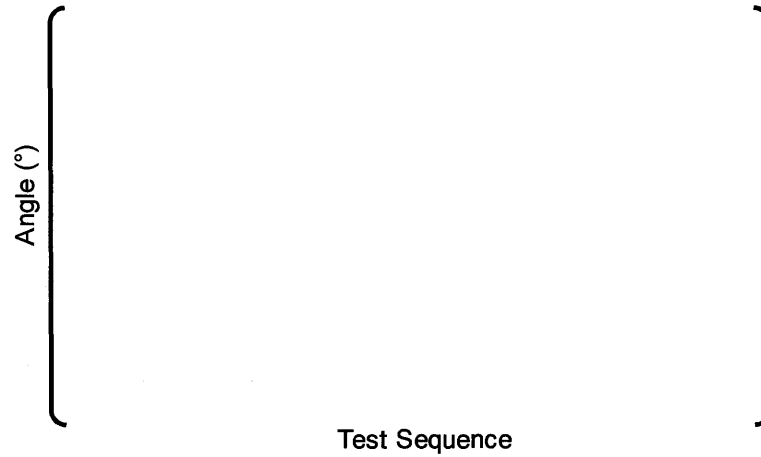


Figure 4.2.1-4 Variation of Pendulum Angle in Simulation Test Cases

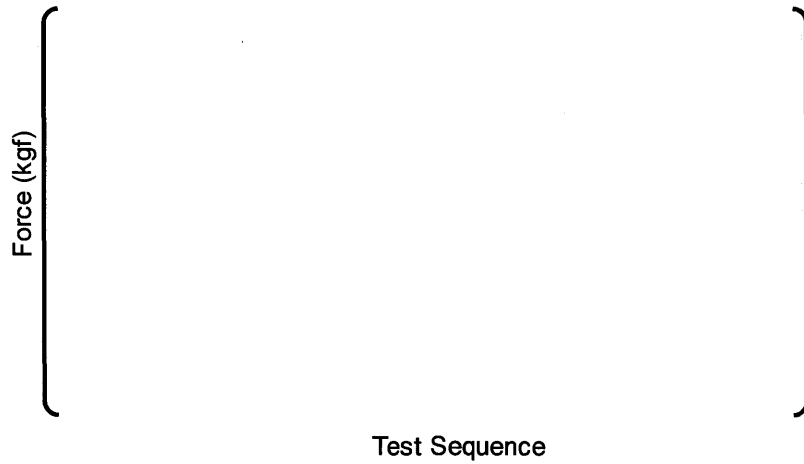


Figure 4.2.1-5 Comparison of Analyzed and Measured Impact Force

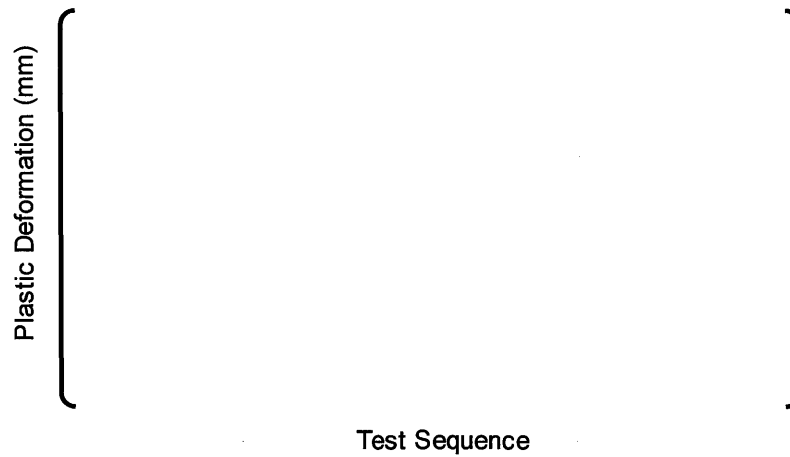


Figure 4.2.1-6 Comparison of Analyzed and Measured Plastic Deformation

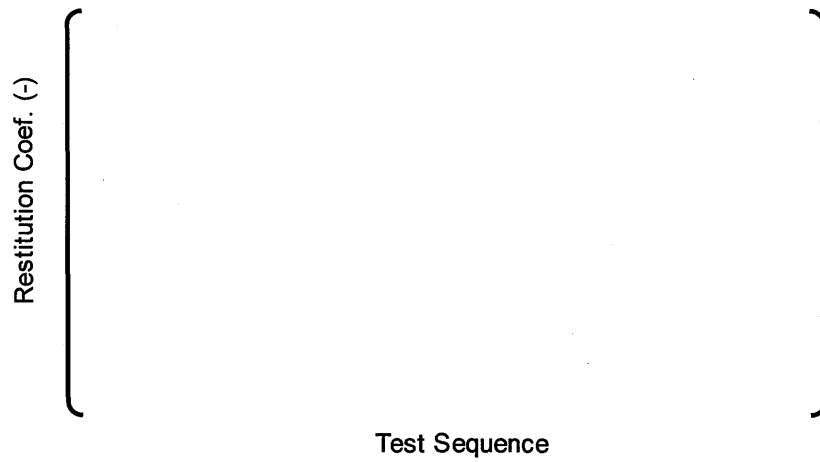


Figure 4.2.1-7 Comparison of Analyzed and Measured Restitution Coefficient

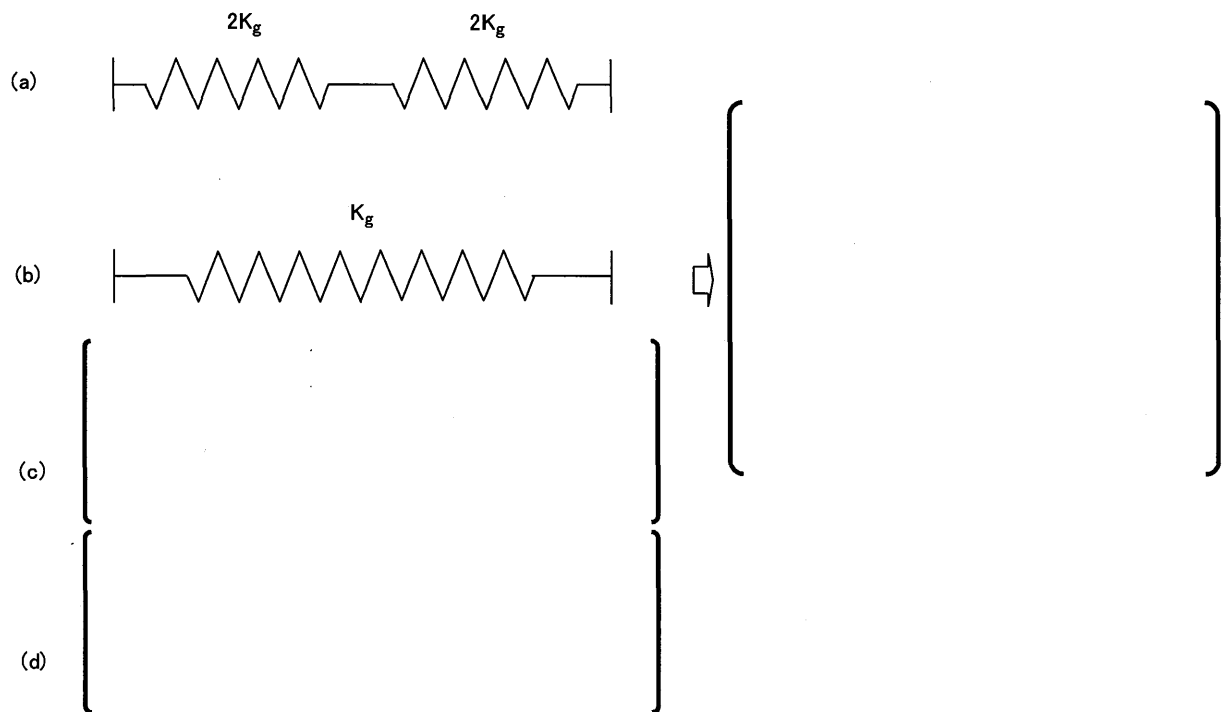
4.2.2 Characteristics for Half-sized Grid Spacer Region

The elastic-plastic impact model for a full-sized grid spacer is described in the previous section. The model needs to be changed for a half-sized grid spacer for use in the FINDS code. There are two perspectives to correct these values.

CASE-A : Each half-sized grid spacer behaves symmetrically

CASE-B : Only one side of the grid spacer which buckles first carries the deformation

The following systems are used for determining the model.



[CASE-A]

Set k_s in (c), initially at [] value and then decreasing as buckling progresses, with the total stiffness K_1 given by,

$$K_1 = \left[\quad \right] \quad \dots \quad (4.2.2-1)$$

and the reduced stiffness of the full sized-grid spacer, RSG_{total} is,

$$RSG_{total} = \left[\quad \right] \quad \dots \quad (4.2.2-2)$$

The FINDS code requires the value corresponding to $2K_g$ in (a). If deformation proceeds evenly in both sides of the grid spacer, the model values are ;

$$ESC_{\text{half-A}} = \left[\quad \right] \quad \dots \quad (4.2.2-3)$$

$$DP_{\text{half-A}} = \left[\quad \right] \quad \dots \quad (4.2.2-4)$$

$$RSG_{\text{half-A}} = \left[\quad \right] \quad \dots \quad (4.2.2-5)$$

[CASE-B]

The deformation proceeds as in (d) and the changing stiffness in the half-sized grid spacer, K_2 is,

$$K_2 = \left[\quad \right] \quad \dots \quad (4.2.2-6)$$

A value for K_1 is determined from tests. Using Equation (4.2.2-1), k_s is calculated.

$$k_s = \left[\quad \right] \quad \dots \quad (4.2.2-7)$$

From Equation (4.2.2-6) and the Equation (4.2.2-7), the ratio of K_2 (stiffness of the half-sized grid spacer) and its initial value $2K_g$ is determined.

$$RSG_{\text{half-B}} = \left[\quad \right] \quad \dots \quad (4.2.2-8)$$

For the deformation energy, the following correction is used based on the test data.

$$ESC_{\text{half-B}} = \left[\quad \right] \quad \dots \quad (4.2.2-9)$$

Suppose that deformation occurs in only one side of the half-sized grid spacer,

$$DP_{\text{half-B}} = \left[\quad \right] \quad \dots \quad (4.2.2-10)$$

While there are two perspectives mentioned above, looking at actual buckling behavior it can be judged that the deformation starts with the [CASE-A] pattern and progresses to a [CASE-B] pattern. Thus, in the FINDS code the following transformation is adopted.

$$ESC_{\text{finds}} = \left[\quad \right] \quad \dots \quad (4.2.2-11)$$

$$RSG_{\text{finds}} = \left[\quad \right] \quad \dots \quad (4.2.2-12)$$

$$DP_{\text{finds}} = \left[\quad \right] \quad \dots \quad (4.2.2-13)$$

$$\alpha = \left[\quad \right] \quad , \text{ when } \left[\quad \right] \quad \dots \quad (4.2.2-14)$$

$$\alpha = \left[\begin{array}{c} \dots \\ \dots \end{array} \right], \text{ when } \left[\begin{array}{c} \dots \\ \dots \end{array} \right]$$

$$\alpha = \left[\begin{array}{c} \dots \\ \dots \end{array} \right], \text{ when } \left[\begin{array}{c} \dots \\ \dots \end{array} \right]$$

Applying Equations (4.2.2-11) through (4.2.2-14) to the test data, the input for the grid spacer deformation progress in the FINDS code model is obtained as shown in Figure 4.2.2-1 and Figure 4.2.2-2.

As mentioned above, the FINDS code models the occurrence of half-sized grid spacer buckling. Moreover, the actual buckling behavior varies within the half-sized grid spacer. Hence the following additional correction is made.

$$\left(\begin{array}{c} \dots \\ \dots \end{array} \right)$$

For an N x N rod array, expressed by cells of number N, consider the model shown in Figure 4.2.2-3 for the case that it impacts at its left-hand side. The impact load has a distribution due to the distributed fuel rod mass. This model also applies in the case where the impact force is from the left of an adjacent fuel assembly and the force distribution has a trapezoid shape.

The stiffness in each cell is,

$$k_0 = k_N = \left[\begin{array}{c} \dots \\ \dots \end{array} \right], k_i = \left[\begin{array}{c} \dots \\ \dots \end{array} \right]$$

Define the value α using the impact force on the left and right as follows.

$$\alpha = \left[\begin{array}{c} \dots \\ \dots \end{array} \right]$$

The deflection in each cell is given in terms of the deflection of left-hand cell,

$$\delta_0 = \left[\begin{array}{c} \dots \\ \dots \end{array} \right]$$

$$\delta_i = \left[\begin{array}{c} \dots \\ \dots \end{array} \right]$$

The total deflection energy is,

$$E_A^{total} = \left[\begin{array}{c} \dots \\ \dots \end{array} \right]$$

In the right half,

$$E_A^{right} = \left(\quad \right)$$

In the left half,

$$E_A^{left} = \left(\quad \right)$$

On the other hand, the two half-sized grid spacer models are used in the FINDS code, as shown in Figure 4.2.2-4.

The stiffness of each half-sized grid spacer is,

$$k_L = k_R = 2K_g$$

If the deflection at the left side as δ_L , then deflection at the right side is,

$$\delta_R = \left(\quad \right)$$

The deformation energy in the left half is,

$$E_B^{left} = \frac{1}{2} k_L \delta_L^2 = K_g \delta_L^2$$

and the deformation energy in the right half is,

$$E_B^{right} = \frac{1}{2} k_R \delta_R^2 = \left(\quad \right)$$

The deformation progress data used in the FINDS code are obtained from pendulum type tests and it corresponds to the case $\left(\quad \right)$ in this model. In this case, the following equation is satisfied.

$$E_A^{left} = \left(\quad \right)$$

and,

$$\delta_L = \left(\quad \right)$$

Using two types of energy E_A and E_B obtained from the two models above, define the value β , $\beta = \left(\quad \right)$ as a function of a , then β increases with decreased a . By using this $\beta = func(a)$, the correction from two half-sized grid spacer models in the Figure 4.2.2-4 to the multiple division models in the Figure 4.2.2-3 can be made. The calculated half-sized grid spacer deformation energy E_B^{left} is corrected to $\left(\quad \right)$. It is then compared with grid spacer deformation progress data and after that the evaluation of buckling is made to simulate the actual buckling behavior more precisely.

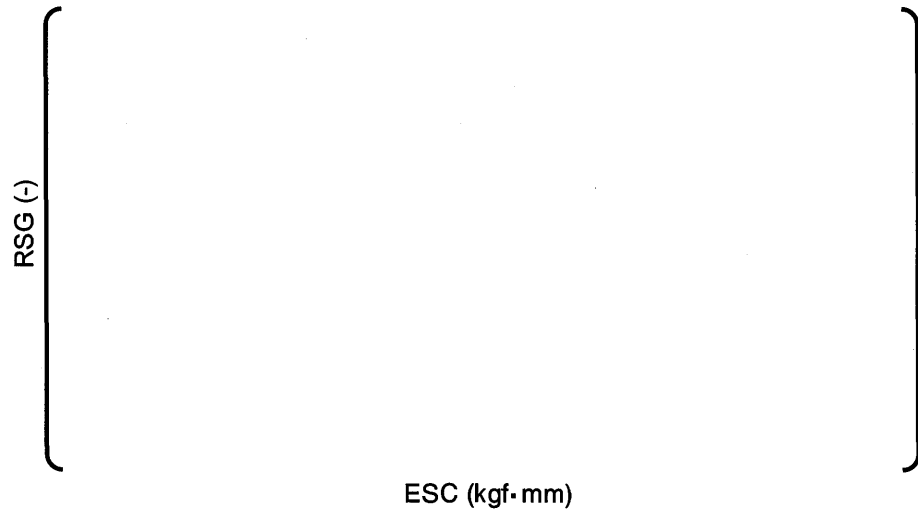


Figure 4.2.2-1 Relationship between Reduced Stiffness and ESC for Half-sized Grid Spacer Region

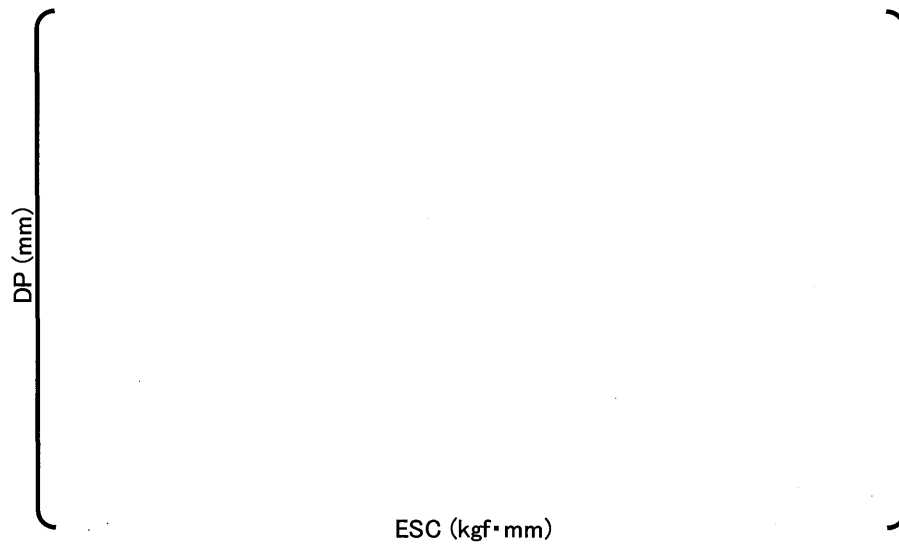


Figure 4.2.2-2 Relationship between Plastic Deformation and ESC for Half-sized Grid Spacer Region



Figure 4.2.2-3 Force Distribution among Sequential Grid Spacer Cells



Figure 4.2.2-4 Deformation Distributions in Grid Spacer Model

final amplitude dependence of the natural frequency is shown as "std-hot" in Figure 4.3-2.

(4) Impact stiffness of grid spacer

The test in hot conditions is preferable for this characteristic. In particular, in the case of Zircaloy-4 grid spacers for which the material property changes significantly, direct acquisition of hot test data is required. If only cold test data exists, ()

(5) Impact damping

Assuming that the restitution coefficient, ()
()

(6) Grid spacer deformation related characteristics

Material properties, Young' modulus and yield strength affect grid spacer deformation behavior and the data from the hot conditions test is preferable. If only cold test data are available, the following correction for deformation energy is taken.

$$ESC_{hot} = ()$$

where

$$C_1 : ()$$

$$C_2 : ()$$

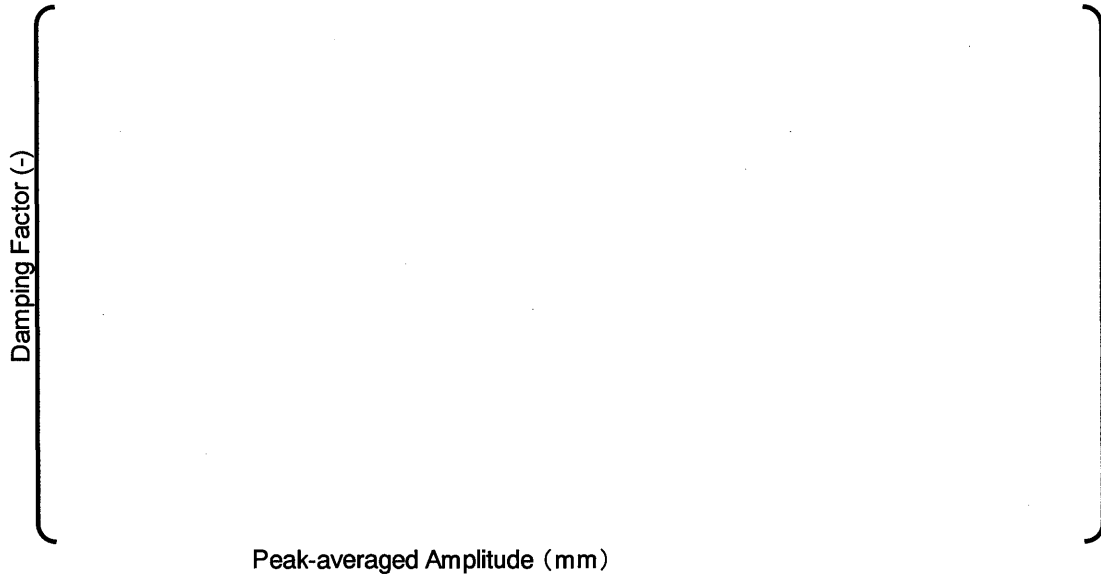


Figure 4.3-1 Damping Factor at Hot Conditions

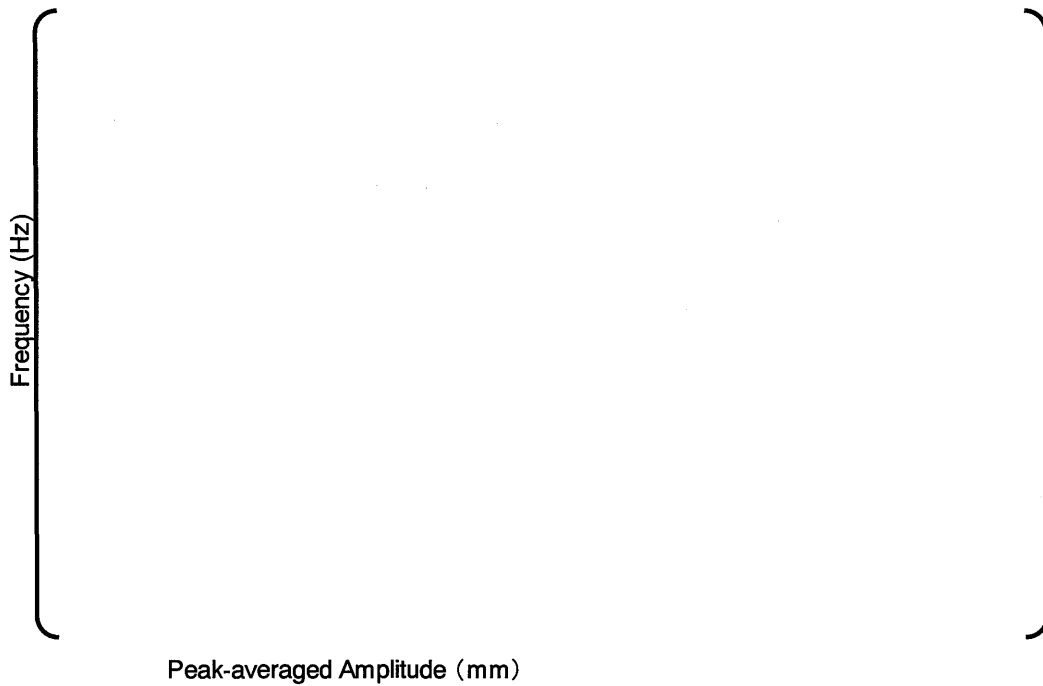


Figure 4.3-2 Natural Frequencies at Hot Conditions

5.0 VERIFICATION OF THE FINDS CODE

5.1 Vibrational Behavior of the Beam Model

In order to verify the beam model used in the FINDS code, vibration analyses of a single beam have been done with the FINDS code and the general finite element method code ANSYS.

The models used in the analyses are fundamentally same as the fuel assembly beam model as illustrated in the Figure 3.2-1 and have following characteristics.

- Beam models in the two codes have [] nodes and [] elements whose mass density and overall length are almost equal to the 17 x 17 fuel assembly with 12 ft active length.
- Impact models of the FINDS code at the grid spacer position do not function because there is no interaction of the single beam. The beam model in the ANSYS code does not contain such impact models.
- [] elements used in the model of the FINDS code can be also modeled by equivalent elements in the ANSYS code.
- Amplitude dependencies of frequency and damping [] [], which are uniquely modeled in the FINDS code, are not used for analytical simplicity. Instead, a constant damping factor of [] is used in the both models.

Three sinusoidal acceleration waves with different frequencies are inputted to the top and bottom ends of the each model. The frequencies correspond to the natural frequencies of the 1st ([] Hz), the 2nd ([] Hz) and the 3rd ([] Hz) mode vibration of the beam model. The magnitude of the acceleration, 1.0×10^3 mm/sec² is the same for all three frequencies.

Figures 5.1-1 through 5.1-3 show the transient response of representative nodal displacements to the different acceleration frequencies. The analysis results from the two codes show good agreement with each other.

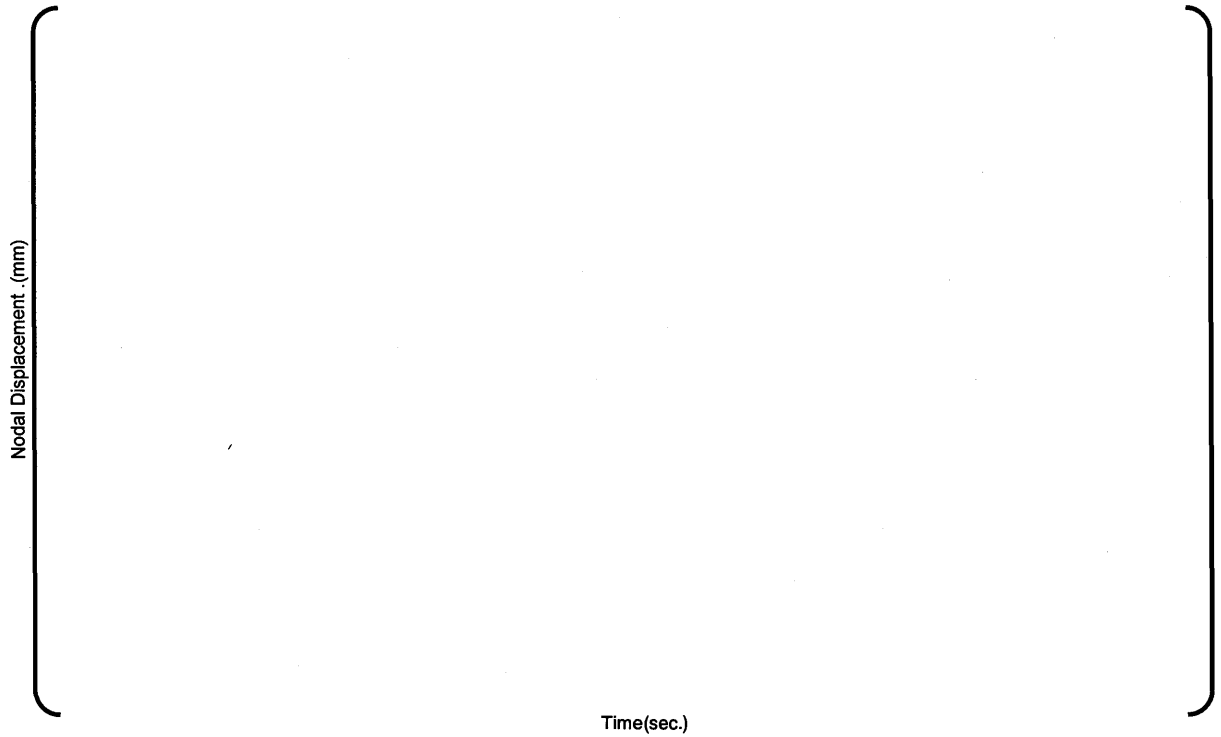


**Figure 5.1-1 Comparison between FINDS and ANSYS Codes
(Accelerated by the 1st Mode frequency)**

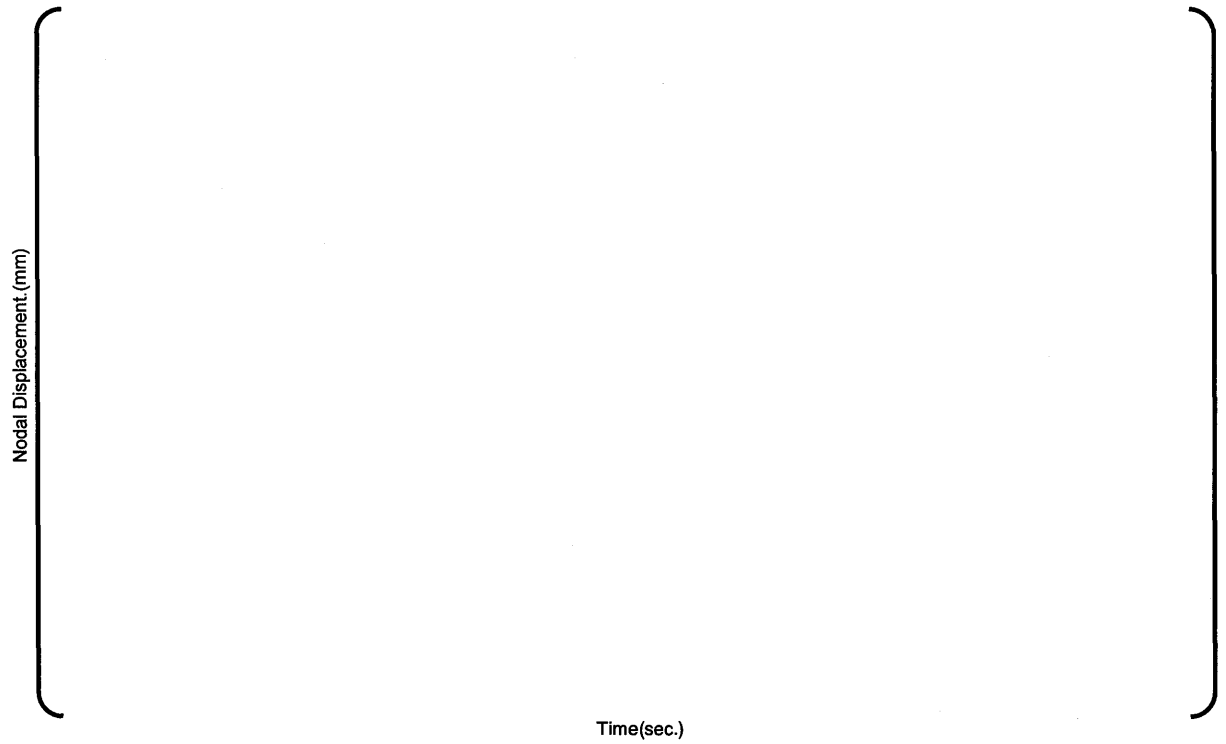


**Figure 5.1-2 Comparison between FINDS and ANSYS Codes
(Accelerated by the 2nd Mode frequency)**

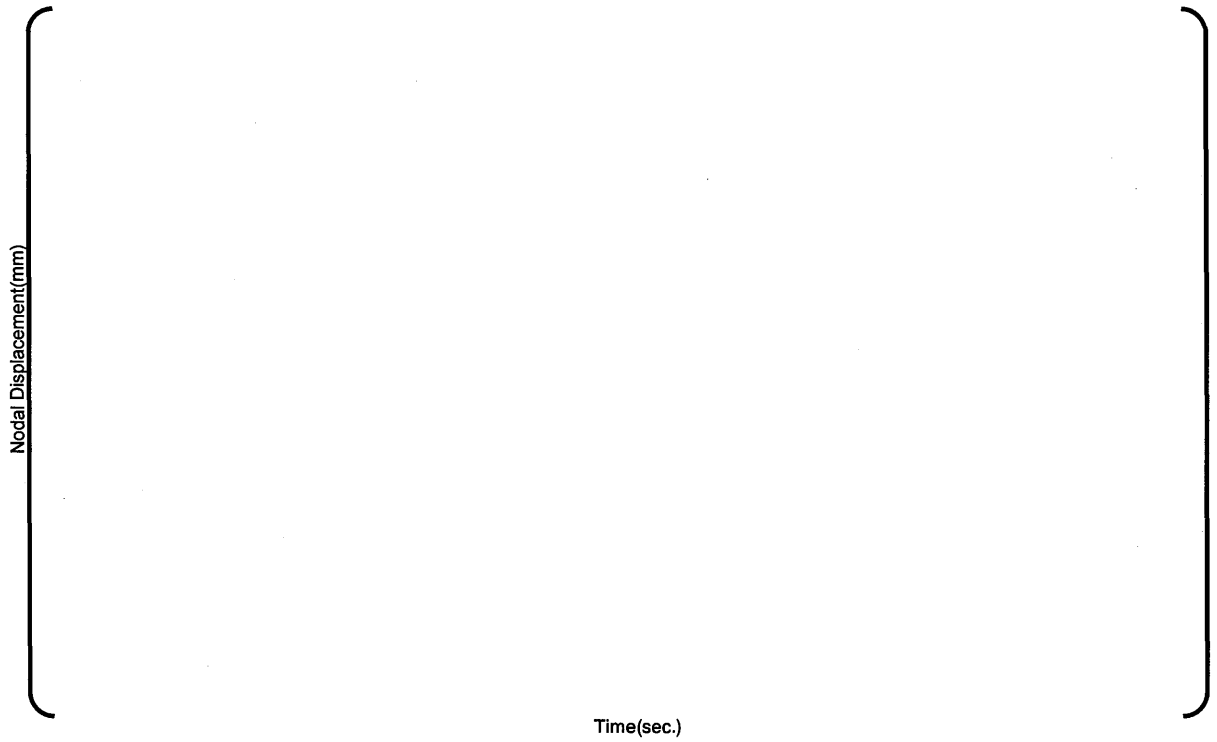


**Figure 5.1-3 Comparison between FINDS and ANSYS Codes
(Accelerated by the 3rd Mode frequency)**

5.2 Lateral Impact Test of Fuel Assembly

The lateral impact tests (pluck tests with a frontal rigid wall) using a full-scaled mock-up fuel assembly of a conventional 17x17 type, 12ft active length were conducted in air to confirm the adequacy of the non-linear vibration model and the impact model. The impact forces at three grid spacer elevations (4th, 5th and 6th from top) and the displacement at the 5th grid spacer were measured after releasing an initial displacement of up to () mm at the 5th grid spacer. The analyses for each test condition were performed using the FINDS code to simulate initial displacement given by the 1st modal displacement of the fuel assembly beam model.

Figure 5.2-1 shows the comparison of experimental impact forces and calculated ones using the FINDS code. Figure 5.2-2 shows the measured and calculated first rebound displacements at the center (5th) grid spacer in each test condition. The calculated results (impact forces and rebound displacements) agree well with the experimental ones.

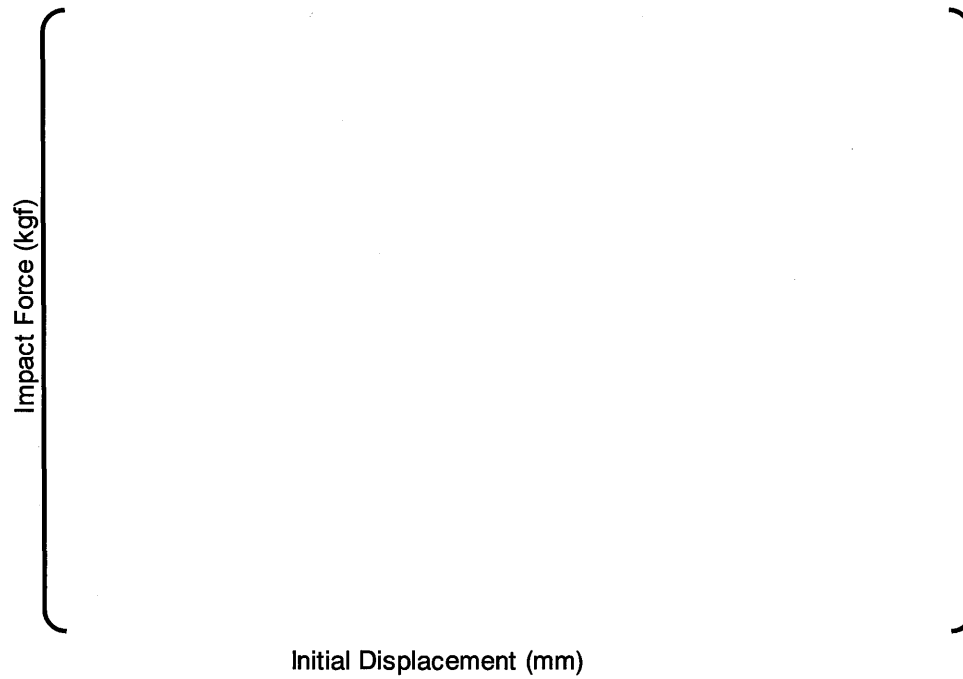


Figure 5.2-1 Impact Force

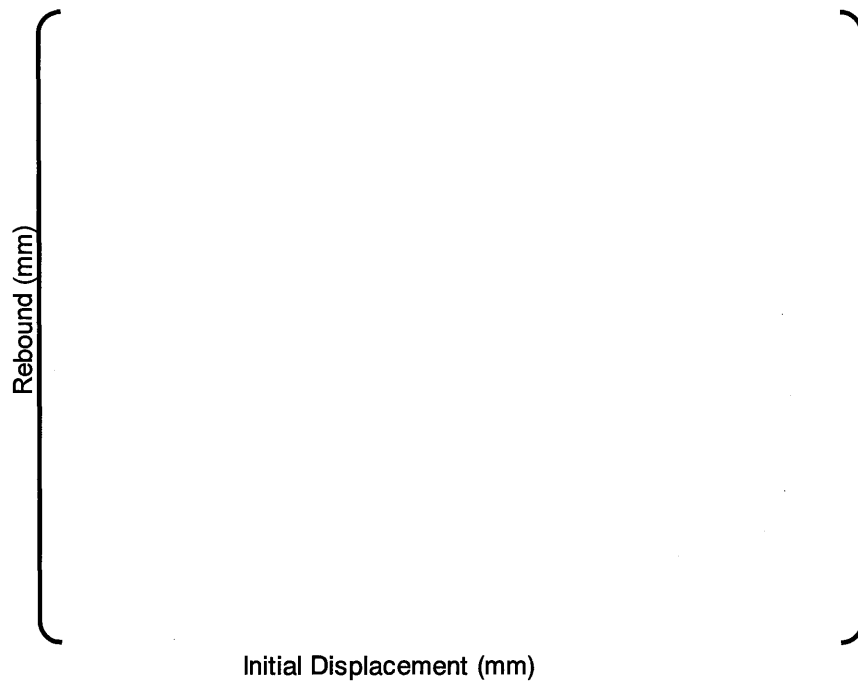


Figure 5.2-2 Rebound Displacement

5.3 Impact Tests of Single Span Fuel Assembly

In order to verify the in-elastic impact model in the FINDS code, special fuel assembly impact tests were conducted, as shown in Figure 5.3-1. Test samples of a single span fuel bundle (with a grid spacer) were dropped onto a rigid foundation. By this type of test, one obtains grid spacer deformation characteristics of a double-sided impact but also takes into account the distributed mass of the fuel assembly, and it can include the higher mode effects that are very important for the impact behavior. A "grid spacer and pendulum" type impact test is also a double sided impact but does not include []. In the single-sided test, the weight attached to the test sample simulates the back side mass effect of the adjacent fuel assemblies occurring in the multi-fuel assemblies' collision condition. In the test the drop height was gradually increased.

The calculated results using FINDS are compared with the measurements. [] drop tests were conducted where the drop height was increased from [] mm to [] mm. Figure 5.3-2 gives the correspondence between the drop heights and the test sequence. The impact load and rebound height were measured in each test. The buckling deformation was also measured after each impact.

The changes in impact load, deformation and restitution coefficient are compared between the tests and the analysis as shown in Figure 5.3-3 through Figure 5.3-4. The restitution coefficient is defined as follows.

$$e = \sqrt{H_r / H_i} \quad H_i : \text{drop height,} \quad H_r : \text{rebound height}$$

In the analysis, in the [] test, the restitution coefficient quickly decreases, the impact load reaches a maximum and inelastic deformation starts at the [] sequence, which agrees well with the test results. The changes in load, deformation and restitution coefficient after the [] sequence are also in good agreement

Based on these results, the adequacy of the inelastic model has been verified.

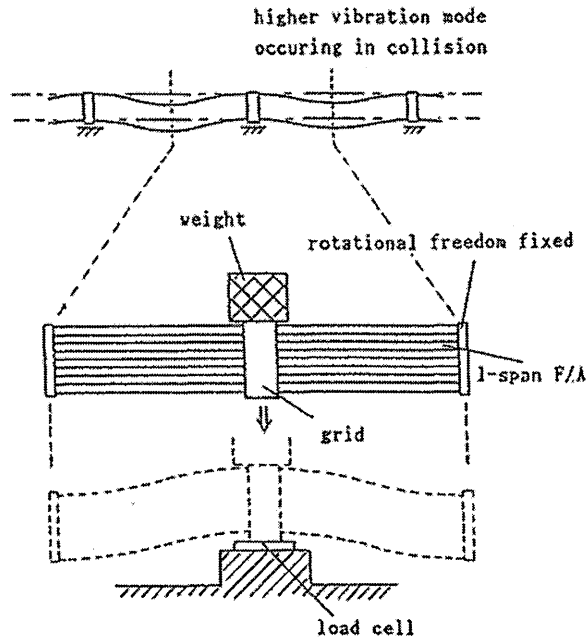


Figure 5.3-1 Single Span Fuel Assembly Impact Test

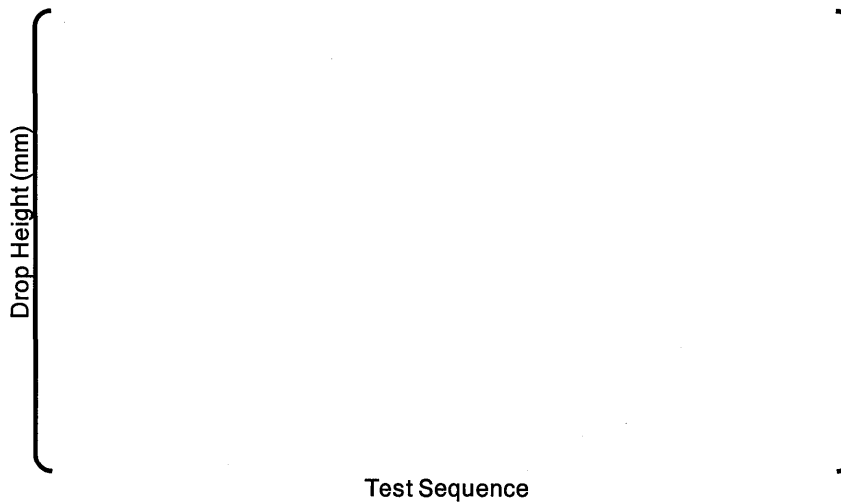


Figure 5.3-2 Drop Height of the Single Span Fuel Assembly

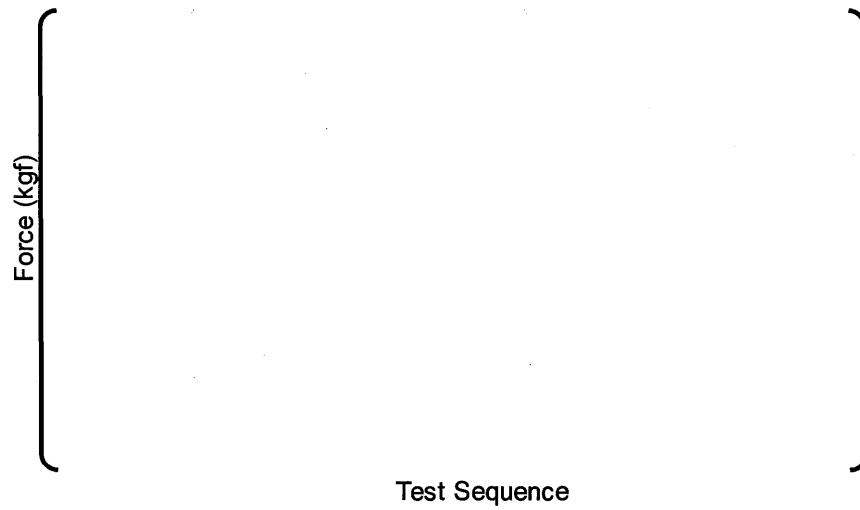


Figure 5.3-3 Comparison of Calculated Impact Forces with Measurements

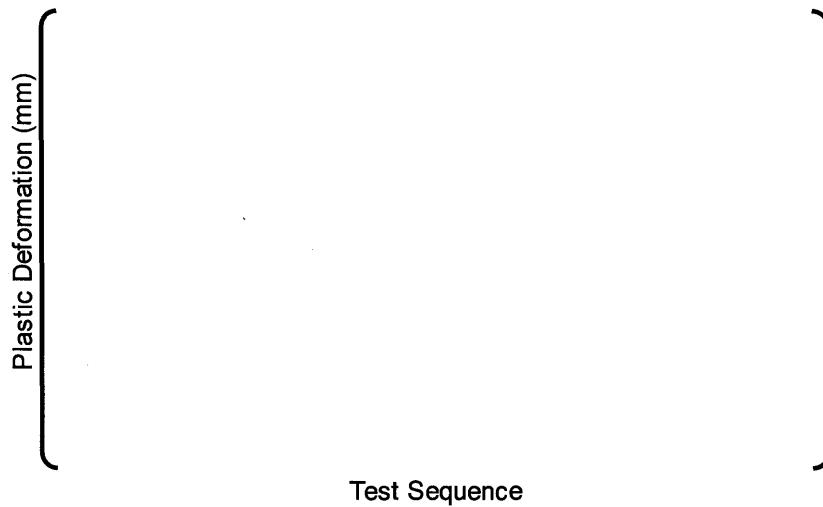


Figure 5.3-4 Comparison of Calculated Deformation of Grid Spacers with Measurements

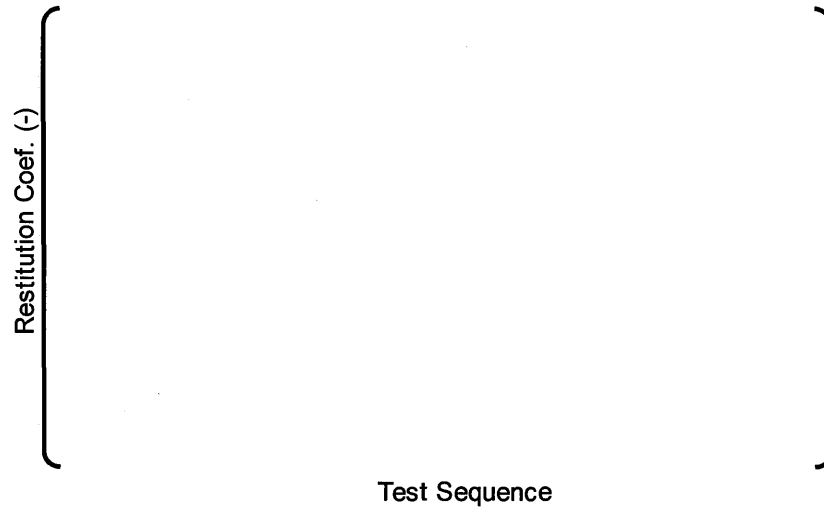


Figure 5.3-5 Comparison of Calculated Restitution Coefficient with Measurements

5.4 Seismic Excitation Tests of Multiple Fuel Assemblies

In order to examine the seismic response of major components in the nuclear power plant, a large scale high-performance shaking table was constructed and reactor vessel, piping, pressure vessel and core internals were tested using this table. The test was sponsored by the Japanese government and the test of PWR core internals was performed from 1981 through 1985. Reference 4 summarizes the tests. The magnitude of the seismic wave was chosen to cover the most limiting earthquake expected in Japan. The test includes the evaluation of the seismic analysis methods.

The test for PWR core internals was performed using a full-scale model of 100 MWe class PWR core internals. This test was chosen to simulate the vibration behavior of the reactor core region and control rod insertion function.

The major components of the test model are a maximum of 45 mockup fuel assemblies of the Mitsubishi conventional 17 x 17 type with a 12ft active length, 2 rod cluster control assemblies, 2 guide tubes, 2 control rod driving mechanisms (CRDMs) and core support structure including a lower core support structure, upper core support structure, vessels and upper structure. The configuration of the test model is shown in Figure 5.4-1. Fuel assemblies in the core are arrayed in three ways, 7x1, 7x7, and 15x3. 7x1 and 7x7 were used to study the effect of the number of fuel assemblies, and the effect of the direction of the wave input parallel or diagonal to the fuel array. The verification test was performed using a 15x3 array and fuel assemblies' behavior under earthquake such as fuel assemblies' response with collision with each other or control rod insertion was checked.

Fuel assembly response and control rod insertion under expected seismic conditions were checked using the 15x3 array. As the basic design earthquake ground motion waves, S_1 and S_2 , which had been approved and standardized by the Japanese regulatory authority as nuclear plant design waves for the high seismic zones, were used.

The result from the S_1 wave test described in Reference 4 was compared with analysis using the FINDS code. The acceleration data actually measured at the upper and lower core plate position in the test were used in the analysis. The peak amplitude of the acceleration reached 400 cm/sec². The time history of the displacement generated in the fuel assemblies located at both ends of the row are shown in Figure 5.4-2 with their analysis result using the FINDS code. The maximum displacement and the maximum impact force generated in these assemblies are shown in Figure 5.4-3 and Figure 5.4-4 compared with their analysis result. The measurement and analysis agreed fairly well. The vibration behavior of the 15 fuel assemblies at the 5th grid spacer elevation (the center grid spacer within the 9 grid spacers) calculated by the FINDS code during S_1 is shown in Figure 5.4-5.

The input list for the analysis mentioned above is attached as Appendix A which also contains an explanation and concrete values of major input variables. An outline of the corresponding output list is also attached as Appendix B.

The result from the S_2 wave test described in the Reference 4 was also compared with its analysis result. In this test the seismic acceleration level was almost two times that of the S_1 case. As the impact forces generated at some grid spacer elevations of the fuel assemblies at both ends of the row exceeded its elastic limit, the dimensional changes of some grid spacers, which reached about 2 mm maximum, were observed after unloading the fuel assemblies. The time history of the calculated impact forces and the dimensional change ("deformation") of

the 5th grid spacer of outermost fuel assemblies are shown in Figure 5.4-6. The analysis indicates the grid spacer deformation had progressed step by step after initiation after about 7 seconds when the highest impact force was generated. The calculated maximum deformation of grid spacers is about 2.2 mm at the center grid spacer elevation of both ends of the row. This result agrees well with the measured one.

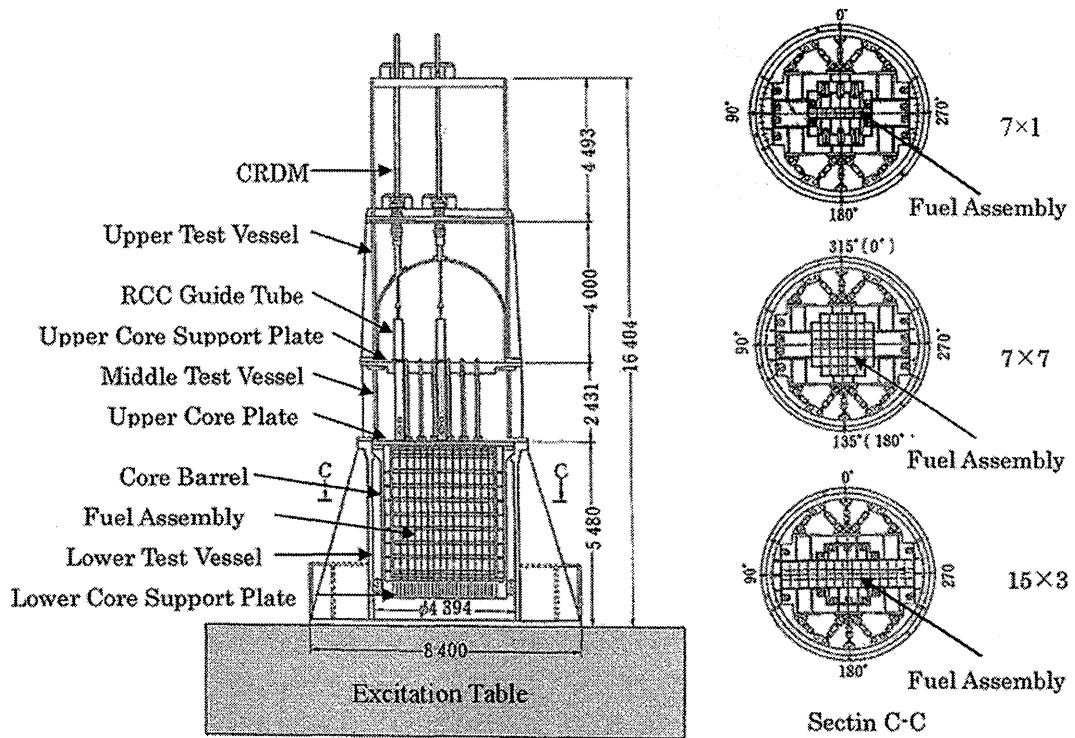


Figure 5.4-1 Configuration of PWR Core Internals Seismic Response Test

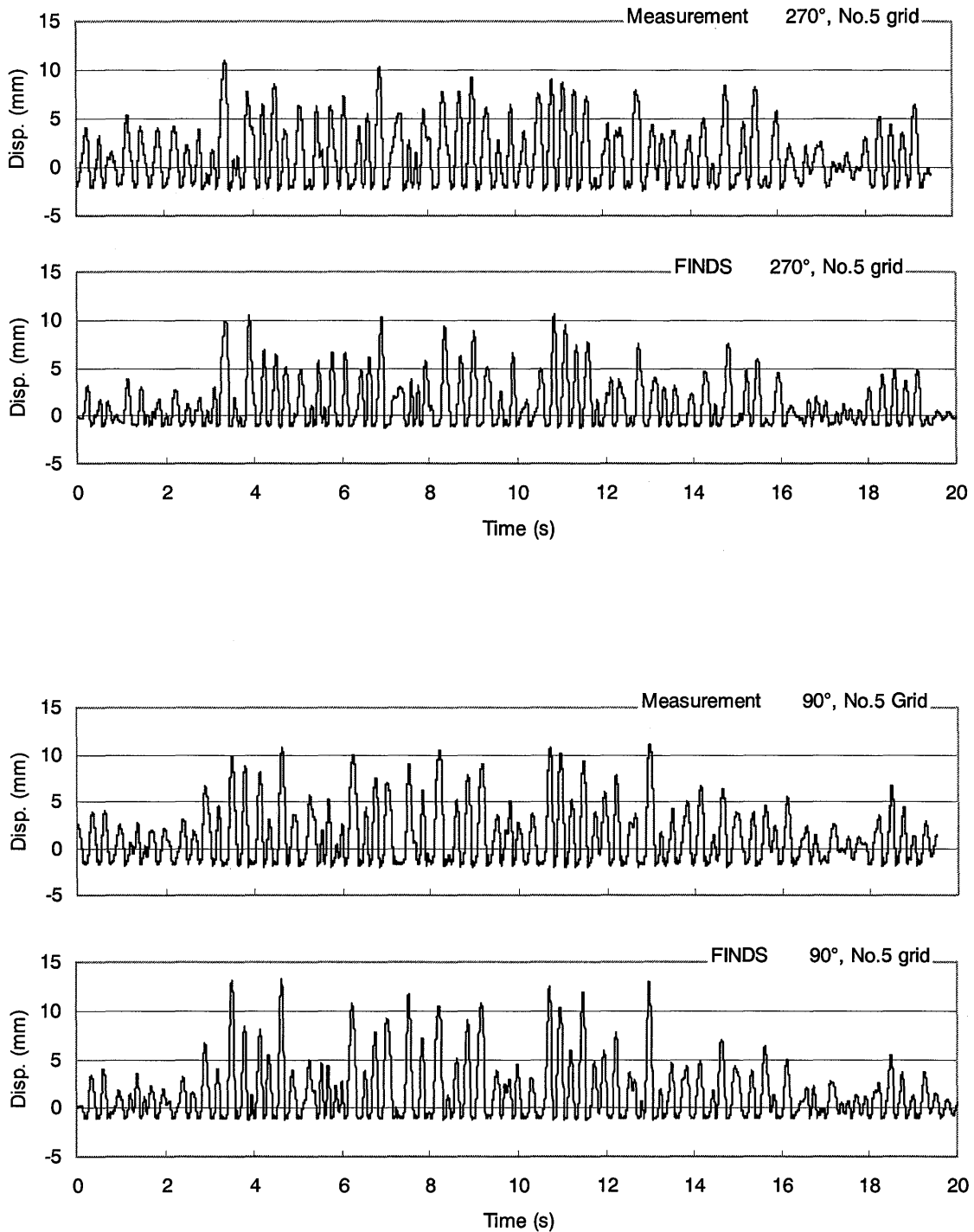


Figure 5.4-2 Displacements of the Fuel Assemblies at Both Ends of the Row

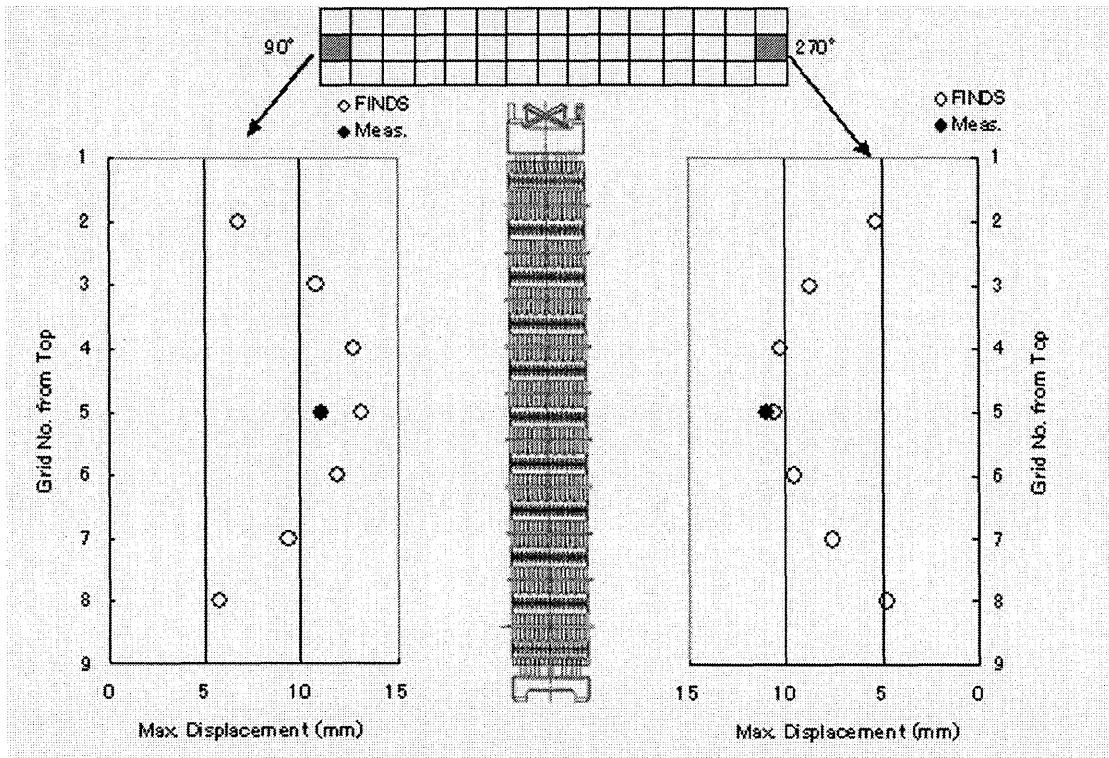


Figure 5.4-3 Grid Spacer Maximum Displacement (S₁ Wave)

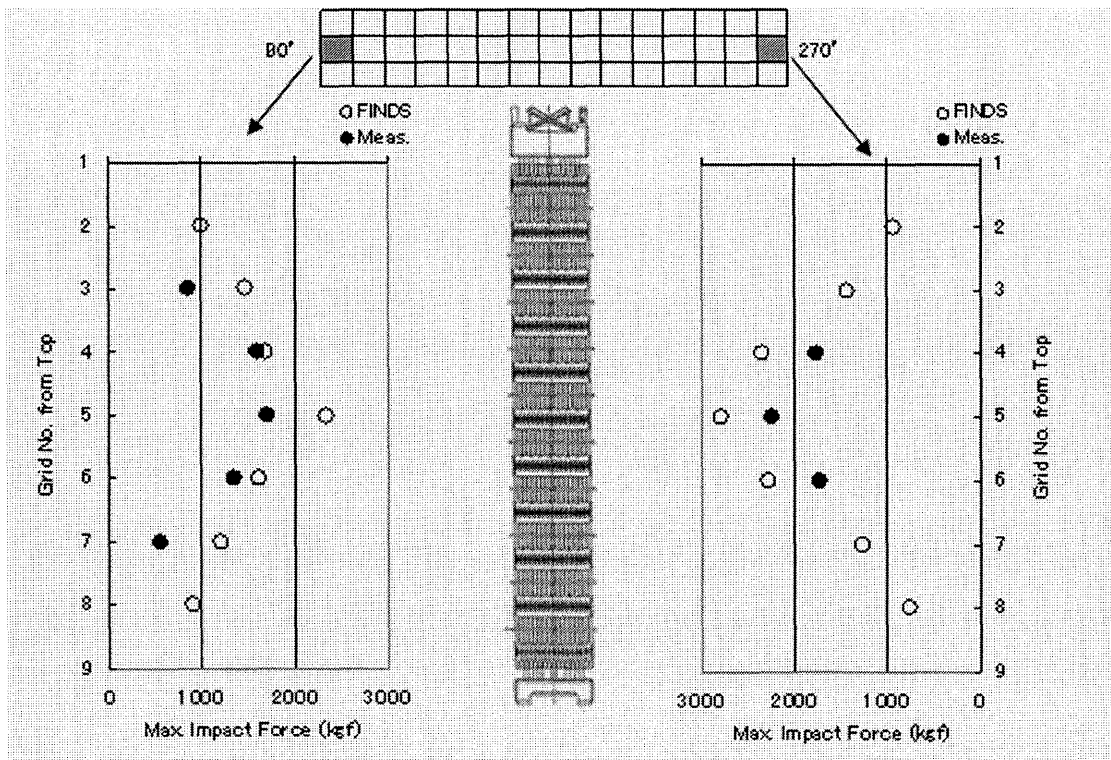
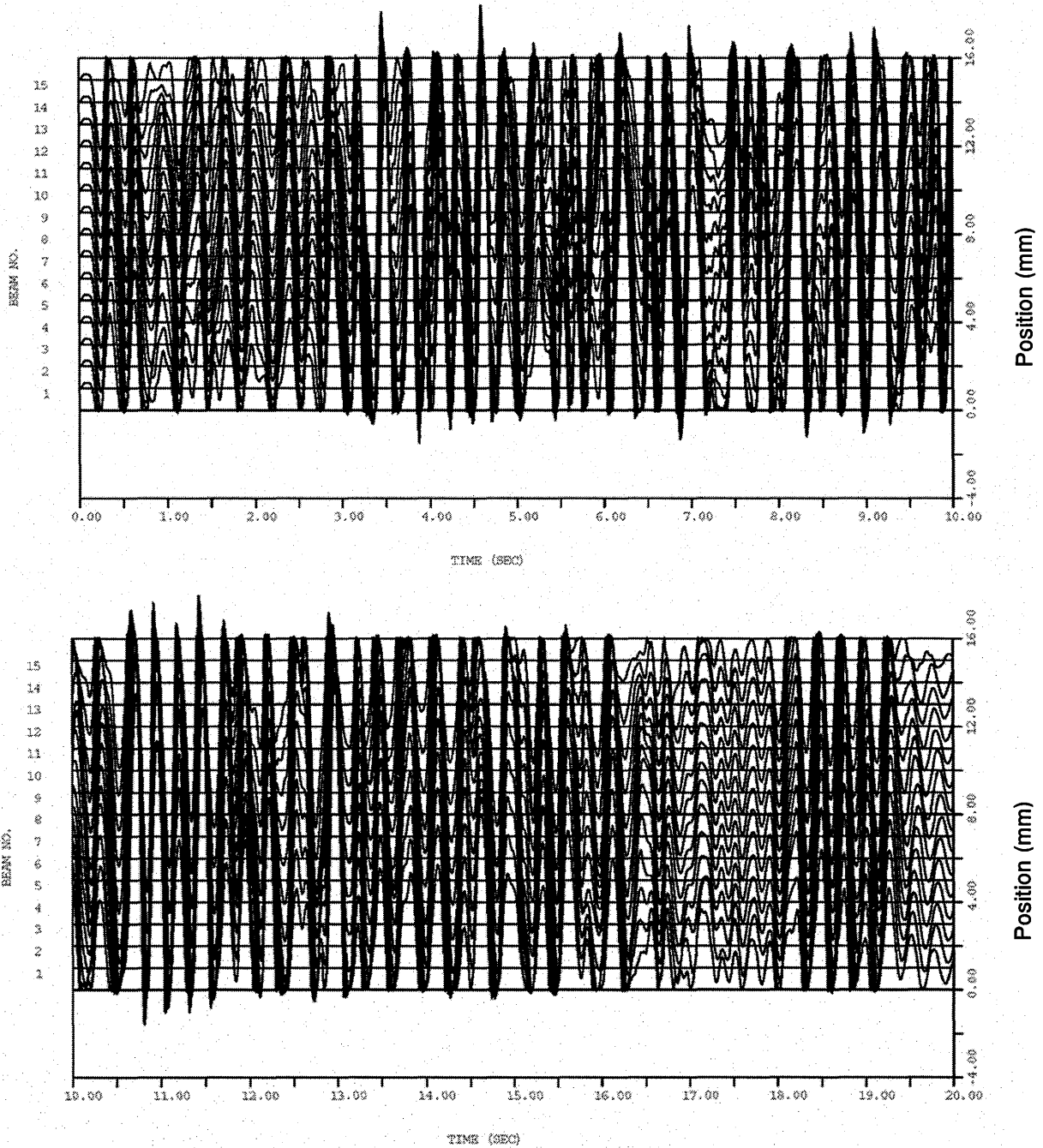


Figure 5.4-4 Maximum Impact Force on the Fuel Assembly (S₁ Wave)



**Figure 5.4-5 Vibration Behavior of the Multiple Fuel Assemblies
(Time History, 0-20 Seconds, S₁ Wave)**

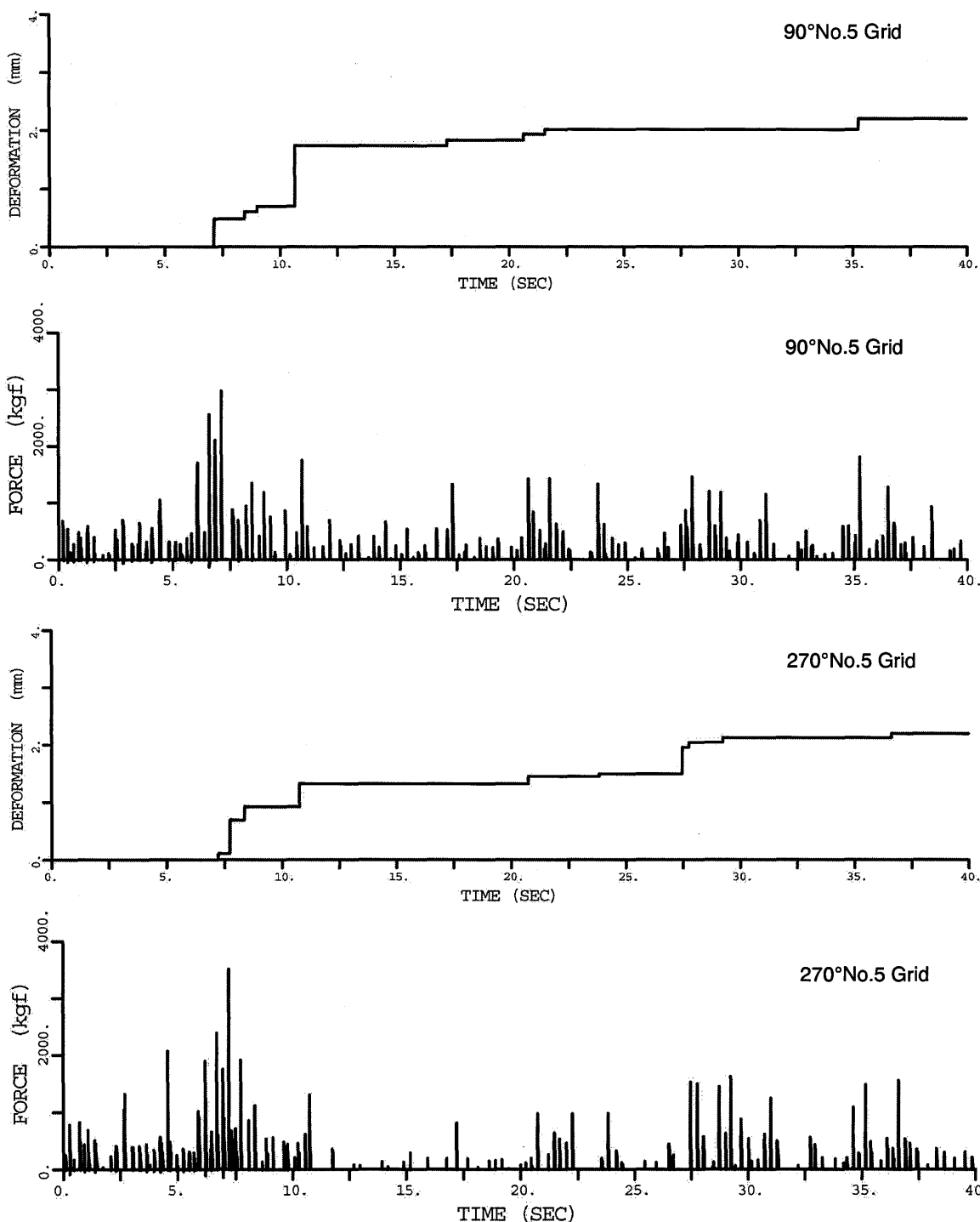


Figure 5.4-6 Impact Forces and Grid Spacers' Plastic Deformation in the Fuel Assemblies at Both Ends of the Row (S₂ Wave)

6.0 CONCLUSION

Mitsubishi has developed the FINDS code for PWR fuel assembly seismic analysis. The code predicts the behavior of the fuel assemblies in a PWR core under seismic conditions such that lateral vibration results in large amplitudes and collision with each other at their grid spacer locations. Both theoretical and empirical models are used in the FINDS code to simulate unique characteristics in the vibration response of the fuel assembly and impact of the grid spacers. The models were adjusted using experimental data obtained by the fuel assembly lateral pluck tests, and grid spacer impact tests performed with a pendulum and verified by comparison with a general purpose FEM code, and impact tests using full-scale and partial fuel assemblies. Finally, the government sponsored project to examine the seismic response of the PWR core verified the applicability of the FINDS code for the analysis of multiple fuel assembly vibration and interaction.

7.0 REFERENCES

1. Mitsubishi Fuel Design Criteria and Methodology, MUAP-07008-P (Proprietary) and MUAP-07008-NP (Non-Proprietary), May 2007
2. MHI, "Design Control Document for the US-APWR", MUAP-DC020, Rev.0 December, 2007
3. Sato et al., "The FINDS code for Fuel Seismic Analysis Considering In-elastic Impact Behaviors", Application of Modal Analysis to Extreme Loads, ASME PVP-Vol.150, 1988, pp. 29-35
4. H.Akiyama et al., "SEISMIC TEST AND ANALYSIS FOR PWR REACTOR CORE INTERNALS" ASME PVP-1989 Vol.182, SEISMIC ENGINEERING-1989 Design, Analysis, Testing and Qualification Methods

FINDS: Mitsubishi PWR Fuel Assemblies
Seismic Analysis Code

Appendix A
INPUT for FINDS

Non-Proprietary Version

A.0 INPUT for the FINDS Code

The input parameters for the FINDS code are explained using the values shown in Table A-1 which is the input for the analysis described in Section 5.3.

Input to the FINDS code consists of

- Setting the region variables in the analysis
- Title
- Data for the analytical model

A.1 Setting of the Region of the Variables in the Analysis

Input starts with the setting of the region of the variables in the analysis.

In the example, the following region is specified.

NBEAM	MJOINT	NMOD	NMODY	NMODP	KINDBM
()	()	()	()	()	()
MAMP	NESC	NESL	NLIN	NHY	NBMH
()	()	()	()	()	()
NGR	NMODW	KINDGR			
()	()	()			

A.2 Title

Then a case title is input. It can be written on several lines and it ends with 'END'.

A.3 Data for the Analytical Model

Data for analytical model follow. They are divided into several 'CARD' groups.

- CARD1 - CARD6: control of the analysis and output.
- CARD7 - 12, CARD31 and CARD32: input related to grid spacer impact behavior.
- CARD13 - CARD17, CARD27: vibration characteristics of fuel assembly beam model.
- CARD19: reading of earthquake acceleration data.

A.3.1 Input Mainly for the Control of the Analysis and Output.

The expression in ' () ' following a variable name described below corresponds to the abbreviated name listed in Table A-1.

A.3.1.1 CARD1

(1) NBEAM (NB)

NBEAM is the number of fuel assemblies to be analyzed. In general, the fuel assembly array in which the maximum number of the fuel assemblies is included is selected. In the example, NBEAM is 15.

(2) MJOINT (MJ)

MJOINT is the number of nodes in fuel assembly beam model. It includes top and bottom end nodes and in the example MJOINT is [] :

(3) NMOD (NM)

NMOD is the number of modes of natural frequency modes to be analyzed. Natural frequencies and their modal shape up to this number are considered. The FINDS code utilizes the mode superposition method and the vibration modes exceeding this value are not considered in the analysis. In the example case the analysis is done using the [] to the [] modes.

(4) IEXCIT (EX)

IEXCIT defines the type of external force. In the example []
[] .

A.3.1.2 CARD2

(1) KINDBM (KB)

[]

(2) NGR (NGR)

NGR is the number of grid spacers in fuel assembly beam model. In the example the fuel assembly is a 17x17 type fuel assembly with 9 grid spacers and NGR is 7 since the top and bottom grid spacers are not considered in the analysis.

(3) INTERP (IN)

[]

A.3.1.3 CARD2A

•• IGPLST (IGPLST)

IGPLST defines whether an elastic calculation (0) or an elastic-inelastic calculation (1) is done. In the example an elastic- inelastic calculation is specified

A.3.1.4 CARD3

CARD3 is used to input debugging options and has no effect on the analysis.

A.3.1.5 CARD4

•• KB (KB)

[]

A.3.1.6 CARD5

(1) IMPCT (IMPCT)

IMPCT defines the nodes for which impact is considered. In the example, []

(2) JGRID (JGRID)

JGRID designates the nodes which have a grid spacer. In the example, []

A.3.1.7 CARD6

(1) DT (DT)

DT defines the time step for integration in the vibration equation and impact calculation. The units of DT are seconds and in the example the calculation is performed every [] seconds.

(2) FINTIM (FINTIM)

FINTIM is the duration of the calculation. In the sample the calculation continues for [] seconds.

A.3.2 The Main Input Related to Grid Spacer Impact Behavior

The main inputs related to grid spacer impact behavior are described using the example calculation. The explanation for the treatment of in-core conditions is also included.

A.3.2.1 CARD7

- SGRID (SGRID)

SGRID is the dynamic compressive stiffness of the grid spacer during impact and the results from the impact tests are directly used. SGRID corresponds to the k_g in Subsection 3.7.2.

In the example, [] (kgf/mm) is used for the conventional 17x17 type of the grid spacer based on its impact test at hot condition.

In the analysis of in-core conditions, the dynamic stiffness data from impact tests in hot conditions or corrected from data in cold conditions are used, as described in Section 4.3.

A.3.2.2 CARD8

- SROD (SROD)

SROD is the value which corresponds to k_r explained in Subsection 3.7.1 and 3.7.2, and it defines the stiffness of the joint between fuel rod and grid spacer. Its value is defined in terms of a grid spacer's dimples and spring stiffness,

$$SROD = []$$

In the example case, SROD = [] (kgf/mm) is used.

A.3.2.3 CARD9

This card is not presently used.

A.3.2.4 CARD10

- (1) SE (SE)

SE is used to specify the restitution coefficient, []

- (2) CDAMP (CDAMP)

CDAMP is the value that corresponds to 'C' explained in Subsection 3.7.2.

$$K = \left[\right] \text{ (kgf/mm) } \quad \text{(See Figure 3.7-2(b))}$$

M represents the mass of one span length.

$$M = [\quad] \text{ (kgf-sec}^2\text{/mm)}$$

$$C_{Cr} = 2\sqrt{MK} = [\quad] \text{ (kgf-sec/mm)}$$

The restitution coefficient e is,

$$e = \exp\left(-\frac{\zeta\pi}{\sqrt{1-\zeta^2}}\right)$$

Grid spacer impact test data shows that e = [\quad] , then,

$$\zeta = 1/\sqrt{\left(\frac{\pi}{\ln e}\right)^2 - 1} = [\quad]$$

Input CDAMP is

$$C = C_{Cr} \times \zeta = [\quad]$$

[\quad]

A.3.2.5 CARD11

This card is not presently used

A.3.2.6 CARD12

- DELT (DELT)

DELT is the value of the gap between the fuel assemblies and between the peripheral assembly and the core baffle (neutron reflector) at the grid spacer elevation. In the example it is set at [\quad] mm. In the case of a fuel assembly with Zircaloy-4 grid spacers, a larger value of [\quad] mm is used to account for the differential thermal expansion between Zircaloy-4 and the material of the upper core and lower core support plates.

A.3.2.7 CARD31

CARD31 is the data set to define the deformation propagation process of the grid spacer during impact. Figure A-1 explains the detailed procedure. As described in Section 3.7 and 4.2 the data set is obtained from impact and buckling tests using a partial length fuel assembly with one grid spacer. [\quad]

[\quad] . Deformation energy is calculated from the chart of the impact load – deflection curve and the progress of stiffness change and deflection propagation is defined. [\quad]

[\quad] .

A.3.2.8 CARD32

CARD32 is the data input to limit the volume of nodal displacement and grid spacer impact force output.

A.3.3 Main Input Related to Vibration Characteristics of Fuel Assembly Beam Model

The main inputs related to the vibration characteristics of the fuel assembly beam model are described using example calculation. The explanation of the treatment for in-core conditions is also given.

A.3.3.1 CARD13

- ALENG (ALENG)

ALENG is the length of axially divided beam elements. The division of the beam elements is shown in Figure A-2. [



A.3.3.2 CARD14

- (1) AKR (AKR)



- (2) AMASS (AMASS)

AMASS is the mass of [

] . The AMASS inputs are calculated as follows.



[]

[]

[]

[]

(3) YOUNG (YOUNG)

YOUNG is the [] Young's modulus of the beams used in the fuel assembly model to calculate the natural frequencies and vibration modes.

In the example []
[] .

In the analysis []
[] .

(4) AI (AI)

[]

· []

· []

For fuel assembly,

[]

This value is used in the example.

A.3.3.3 CARD15

- H (H)

H is the input to set the structural damping of the fuel assembly beam model for each vibration mode. If amplitude dependence is taken into consideration, some constants described in Section 1.9 should be multiplied by this H value. Values of H from [] to [] are used for the example analysis.

A.3.3.4 CARD16

- FREQ

[]

A.3.3.5 CARD17

[]

[]

A.3.3.6 AKRG (AKRG)

[]

A.3.4 Input Related to Reading of Earthquake Acceleration Data

A.3.4.1 CARD19

(1) DTWAVE (DTWAVE)

DTWAVE defines the time step of the acceleration data at the upper core and lower core support plates in units of seconds. In the example, acceleration data should be read in every [] seconds.

(2) ALPHA (ALPHA)

ALPHA(1) and ALPHA(2) are the multipliers of the acceleration data at the upper core and lower core support plates. The fixed 'mm/sec²' unit for the acceleration is used in the FINDS code, and this variable can convert the units of input acceleration data. In the example the multiplier 10 is specified to convert the 'cm/sec²' input to 'mm/sec²'

(3) NWAVE (NWAVE)

NWAVE is the number of acceleration data points. In the example [] points of data are input.

(4) FMT (FMT)

FMT is the format of acceleration data. In the example the data should be read as 6E12.5 (FORTRAN type).

(5) NCUT (NCUT)

NCUT is the number of the data to be skipped from the beginning. In the example [] .

(6) WNAME

WNAME is the name of the file in which acceleration data at the upper core and lower core support plates are written. In the example the acceleration data should be read from the file named "miti11".

Table A-1 (1) Sample Input File List

Table A-1 (2) Sample Input File List

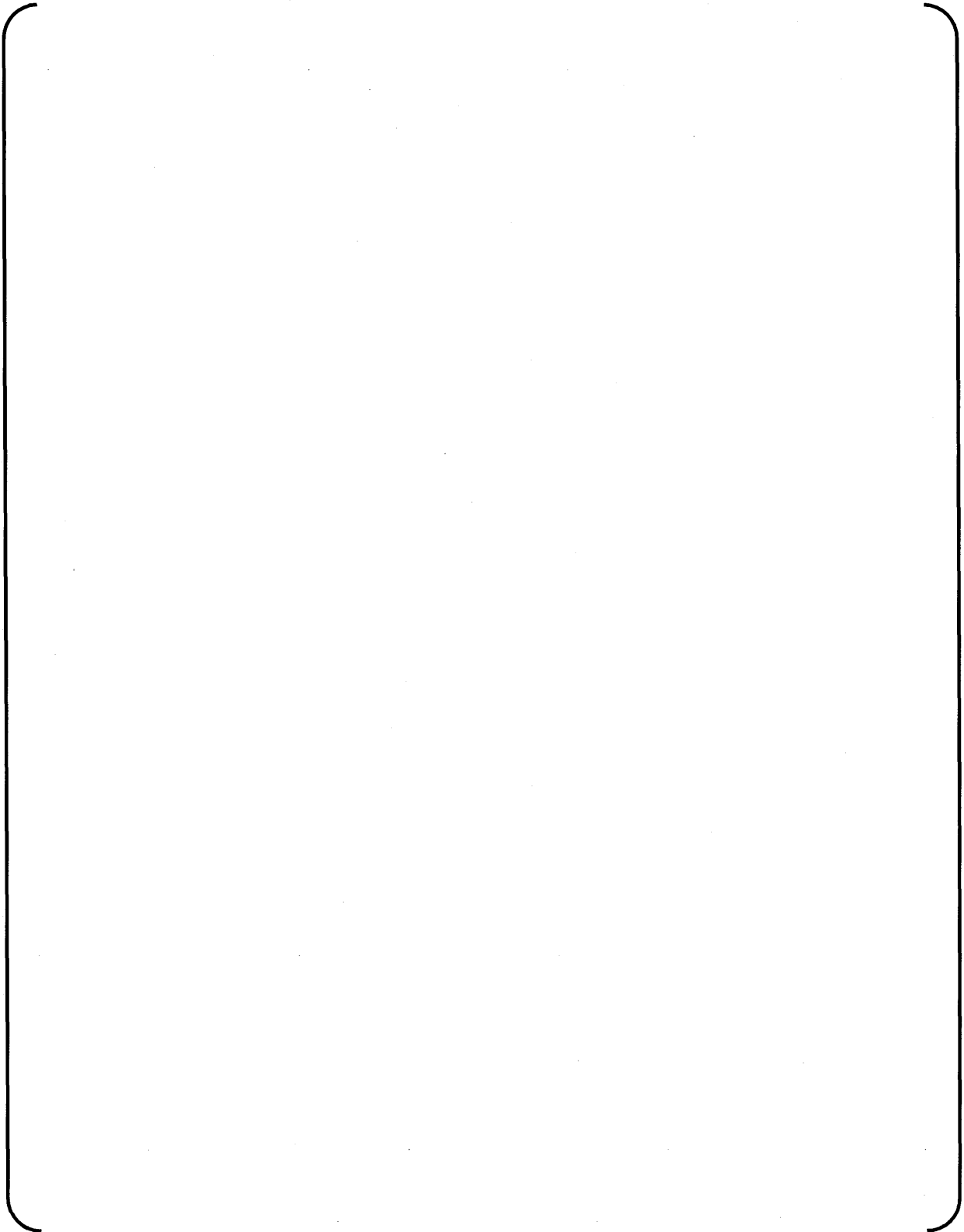


Table A-1 (3) Sample Input File List

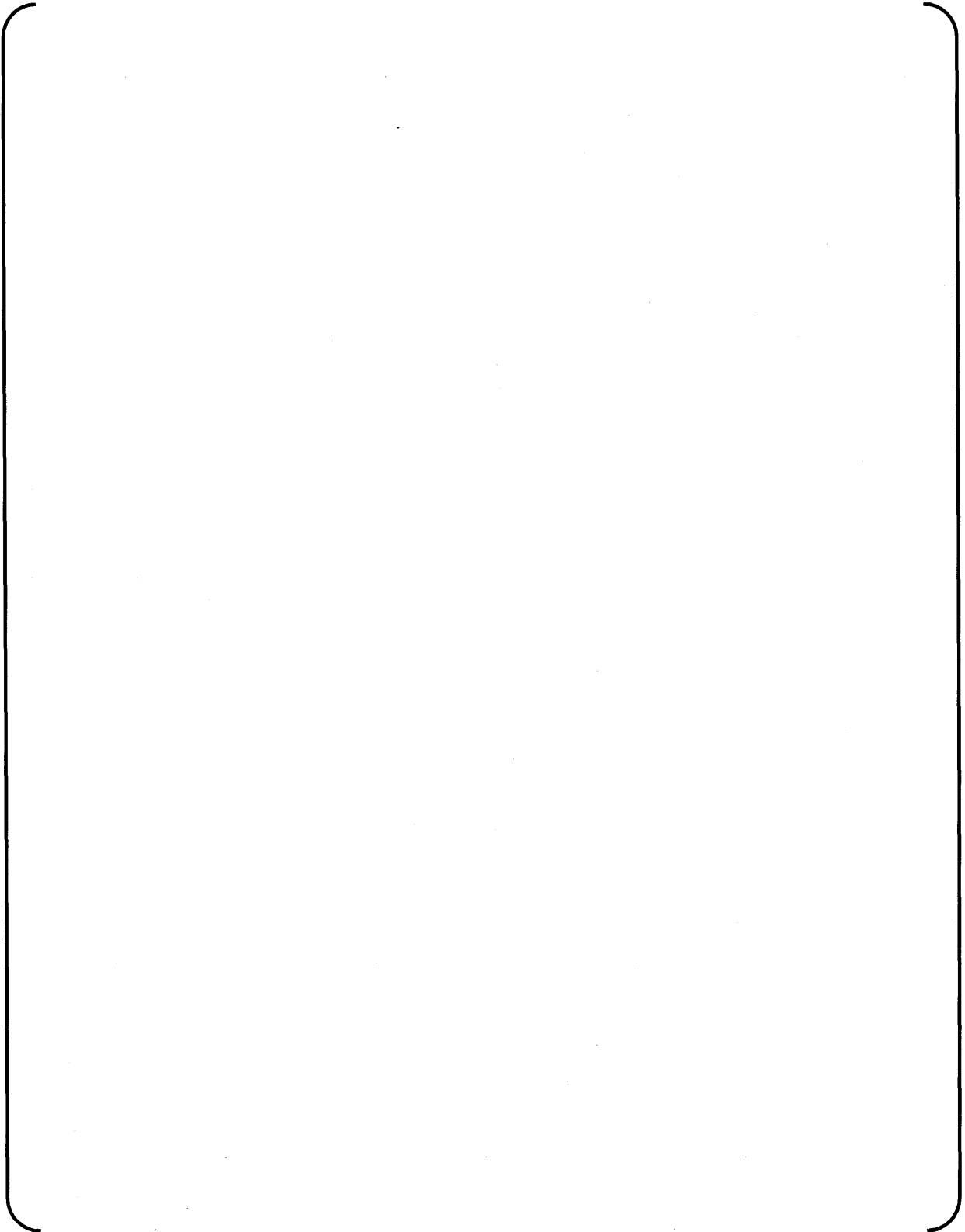
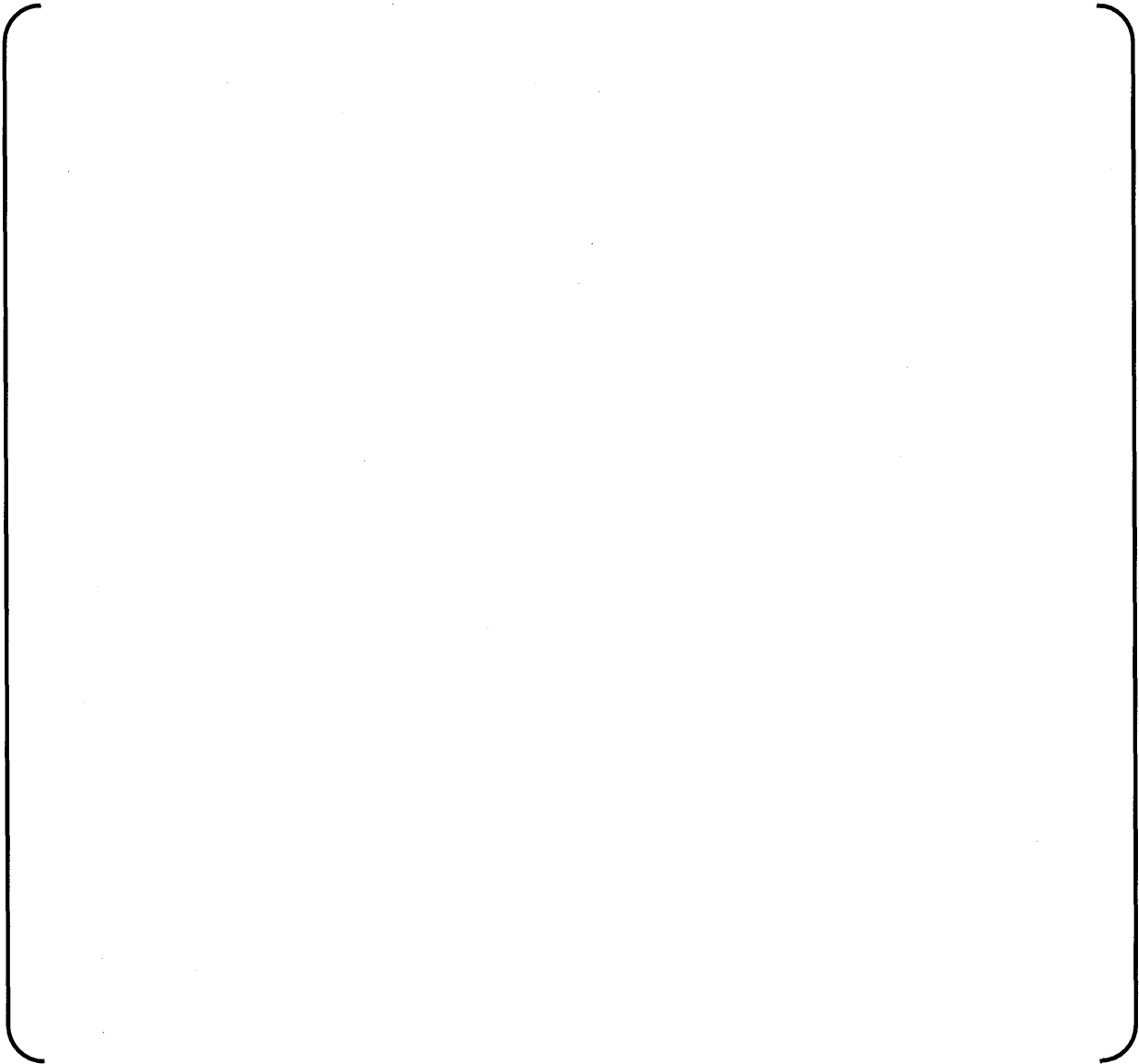


Table A-1 (4) Sample Input File List



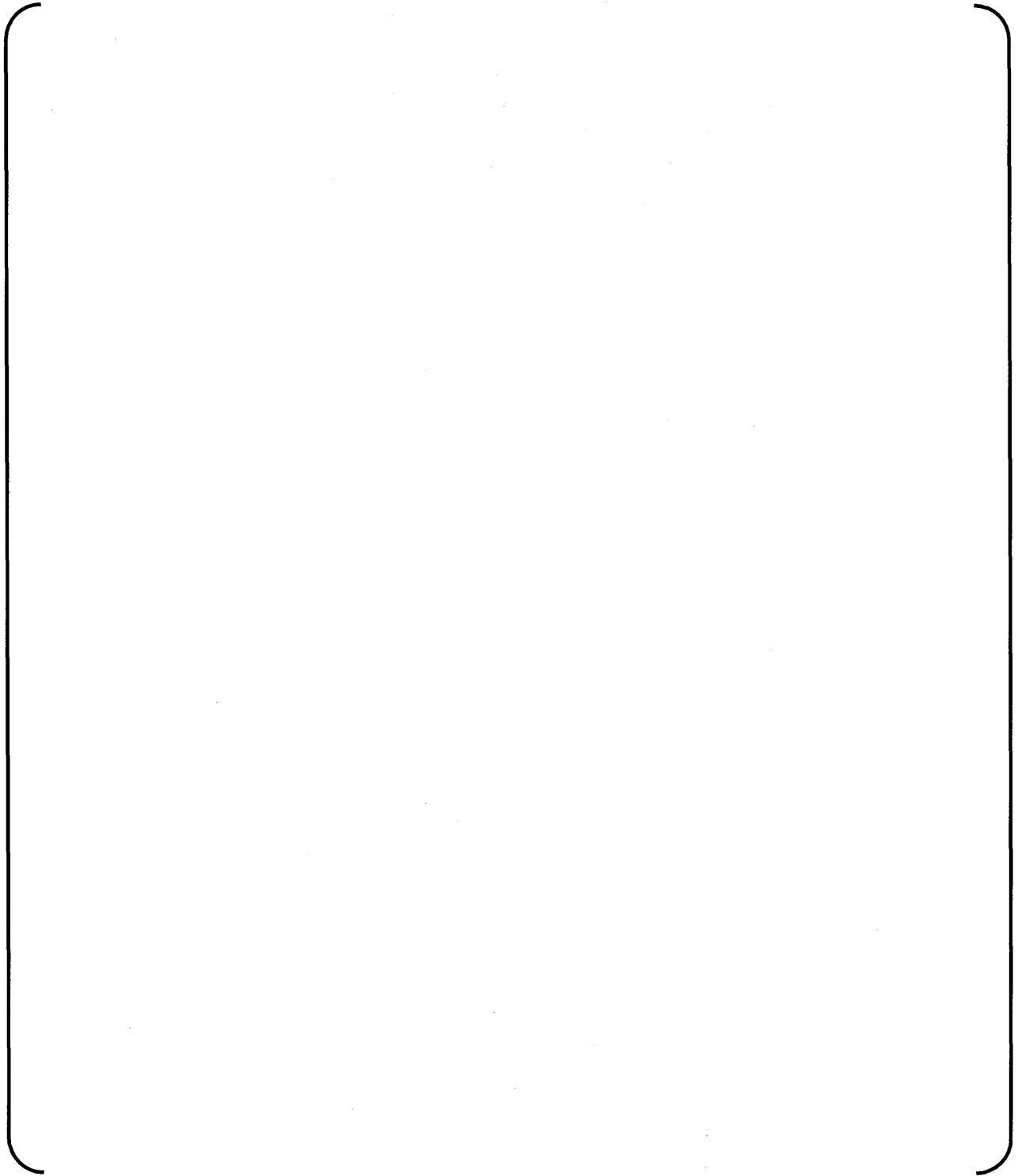


Figure A-1 Description for CARD31

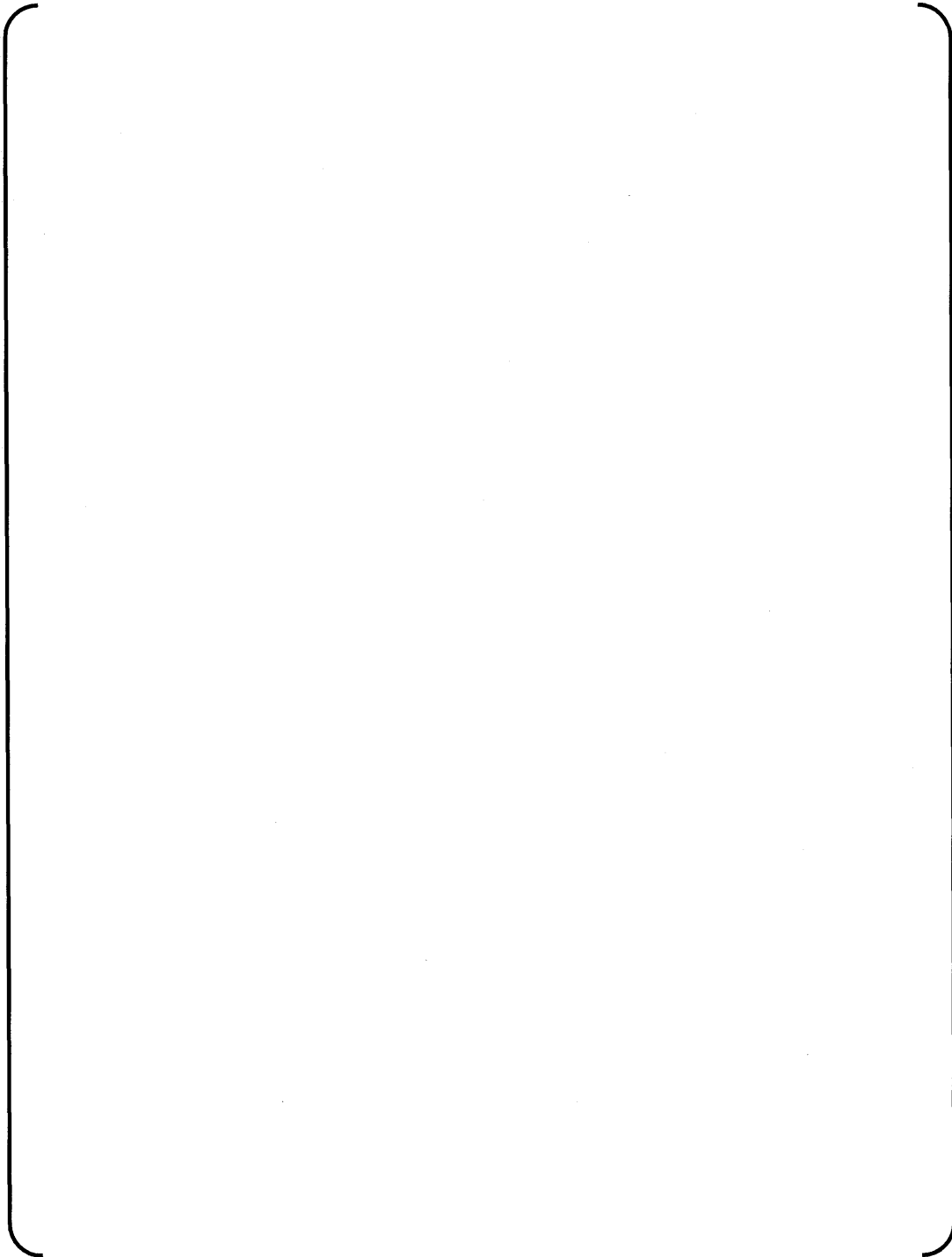


Figure A-2 Element Designations in Fuel Assembly Beam Model

FINDS: Mitsubishi PWR Fuel Assemblies
Seismic Analysis Code

Appendix B

OUTPUT from FINDS

Non-Proprietary Version

B.0 OUTPUT from the FINDS code

Table B-1 selectively summarizes output from the FINDS code which is analyzed to obtain the results described in Section 5.3 based on the inputs in Table A-1 in Appendix A.

Sentences expressed by *Italic* and **bold** letters are added into original output list for explanation.

Table B-1 Input Echo



< Skipped >



Table B-2 Eigen Vector Calculation Results

< Skipped >

< Skipped >

< Skipped >

Table B-3 Undamped Natural Frequency Calculation Results .etc

< Skipped >

<Undamped Natural Frequency>

< Skipped >

Table B-4 Transverse Displacement of Nodes No.1 - 15, at time = 20.0 sec.



Table B-5 Grid Impact Results Summary

[

]

< Skipped >

Table B-6 Maximum Grid Impact Force Summary



Table B-7 Maximum Fuel Assembly Gap Summary



Table B-8 Minimum Fuel Assembly Gap Summary



Table B-9 Maximum Displacement of Fuel Rods Expressed by X in This Report at Each Node



Table B-10 Maximum Displacement of Grid Spacers Expressed by Z in This Report

< Skipped >

Table B-11 Maximum Fuel Rod Force at Grid Spacer Nodes in Each Beam



Table B-12 Maximum Displacement of Rod at Each Node in Each Beam



< *Continued* >

Table B-13 Maximum Displacement of Fuel Rod at Each Node in Each Beam; Continued

< *Continued* >

Table B-14 Modal Components at Maximum Displacement at Each Node in Beam No.1



< *Continued* >

Table B-15 Modal Components at Maximum Displacement at Each Node in Beam No.1 ; Continued

<Continued>



Table B-16 Maximum Displacement at Node for Grid Spacer in Each Beam



Table B-17 Maximum Grid Spacer Deformation in Each Beam



Table B-18 Maximum Storage Energy of Grid Spacer due to Impact in Each Beam

